

Dramatic changes in atmospheric pollution source contributions for a coastal megacity in northern China from 2011 to 2020

Baoshuang Liu^{1,2}, Yanyang Wang^{1,2}, He Meng³, Qili Dai^{1,2}, Liuli Diao^{1,2}, Jianhui Wu^{1,2}, Laiyuan Shi³, Jing Wang³, Yufen Zhang^{1,2*}, and Yinchang Feng^{1,2*}

¹State Environmental Protection Key Laboratory of Urban Ambient Air Particulate Matter Pollution Prevention and Control & Tianjin Key Laboratory of Urban Transport Emission Research, College of Environmental Science and Engineering, Nankai University, Tianjin, 300350, China
²CMA-NKU Cooperative Laboratory for Atmospheric Environment-Health Research, Tianjin, 300350, China
³Qingdao Eco-environment Monitoring Center of Shandong Province, Qingdao, 266003, China

Correspondence to: Y.F. Zhang (zhafox@nankai.edu.cn) and Y.C. Feng (fengyc@nankai.edu.cn)

Abstract

Understanding the effectiveness of long-term air pollution regulatory measures is important for control policy formulation. Efforts have been made using chemical transport modelling and statistical approaches to evaluate the efficacy of the Clean Air Action Plan (2013-2017, CAAP) and the Blue Sky Protection Campaign (2018-2020, BSPC) enacted in China. Changes in air quality due to reduction in emissions can be masked by meteorology, making it highly challenging to reveal the real effects of control measures. Knowledge gap still existed with respect to how sources changed before and after the CAAP and BSPC implemented, respectively, particularly in coastal area where anthropogenic emissions mixed with additional natural sources (e.g., marine aerosol). This work applied a machine learning-based meteorological normalization approach to decouple the meteorological effects from air quality trend in a coastal city in northern China (Qingdao). Secondly, the relative changes in source contributions to ambient $\text{PM}_{2.5}$ with a ~10-year observation interval (2011-2012, 2016, and 2019) were also investigated. We discovered that the largest emission reduction section was likely from coal combustions, as the meteorologically normalized SO_2 dropped by $\sim 15.5\% \text{ yr}^{-1}$ and dispersion normalized SO_4^{2-} decreased by $\sim 41.5\%$ for annual average. Change in the meteorologically normalized NO_2 was relatively stable ($\sim 1.0\% \text{ yr}^{-1}$), and NO_3^- changed inappreciable in 2016-2019 but significantly higher than that prior to the CAAP. Crustal dust decreased remarkably after the CAAP began. Industrial emissions, for example, steel-related smelting, decreased after 2016 due to the relocation of steelmaking enterprises. Note that vehicle emissions were increased in importance, as opposed to the other primary sources. Similar to other mega cities, Qingdao also risks increased ozone pollution that in turns facilitate secondary particles formation in the future. The policy assessment approaches applied in this work also work for other places where air quality management is highly in demand to reduce air pollution.

Key words: Air quality; Random forest; Dispersion normalization; Source apportionment; Coastal megacity

1 Introduction

Rapid industrial development and energy consumption in China over the past several decades have resulted in severe air pollution (Dai et al., 2021; Huang et al., 2014; Zhang et al., 2012). Fine particulate matter (PM_{2.5}, particles with aerodynamic diameter $\leq 2.5 \mu\text{m}$) is the leading health-risk factor for attributable mortality in China (Cohen et al., 2017). It is well-documented that exposure to PM_{2.5} has been associated with increased mortality (Joshi et al., 2021; Liu et al., 2021b; Vodonos and Schwartz, 2021). The World Health Organization recently set the annual average concentration of PM_{2.5} to $5 \mu\text{g m}^{-3}$. Most countries or regions are facing a great challenge now to meet the guideline since their current PM_{2.5} levels are well above the latest threshold.

To alleviate the severe impact of air pollution on the living environment and public health, the State Council of China released a five-year “Air Pollution Prevention and Control Action Plan” in 2013 (hereinafter the “Clear Air Action Plan, CAAP”) (http://www.gov.cn/zwggk/2013-09/12/content_2486773.htm, last access: 29 October 2021). This was followed by the tighter “Three-year Action Plan to the Blue Sky Protection Campaign” (hereinafter the “Blue Sky Protection Campaign, BSPC”) in 2018 (http://www.gov.cn/zhengce/content/2018-07/03/content_5303158.htm, last access: 29 October 2021). The executions of these measures significantly improved air quality (Jiang et al., 2021), thus gained appreciable health benefits (Huang et al., 2018). Vu et al. (2019) demonstrated that the control measures requested by the CAAP have tremendously reduced the emissions in PM_{2.5}, PM₁₀, NO₂, SO₂, and CO in Beijing from 2013 to 2017 by approximately 34%, 24%, 17%, 68%, and 33%, respectively. Xu et al. (2021) found that by 2020, PM_{2.5} reduction measures avoided 3561 thousand morbidity cases and 24 thousand premature deaths in the Beijing-Tianjin-Hebei region.

Evaluation of the effectiveness of air pollution controls is important for control policy formulation to further improve future air quality (Dai et al., 2020). Many studies have been carried out to evaluate the efficacy of control measures around the world. For example, assessments on short-term control measures were made for the 2008 Olympic Games (Schleicher et al., 2012), 2013 Second Asian Youth Games in Nanjing (Qi et al., 2016), 2014 Asia Pacific Economic Cooperation (Xu et al., 2019b), 2015 Military Parade (Wang et al.,

2017), and 2017 Belt and Road Forum for International Cooperation (Ma et al., 2020), as well as the 2020 COVID-19 worldwide lockdown (Beloconi et al., 2021; Chen et al., 2020b; Cucciniello et al., 2022; Shi et al., 2021; Wang et al., 2021a). Medium-term (3–5 years) evaluations on the validity of control measures have also been examined (Li et al., 2021b; Yu et al., 2019; Zhang et al., 2019). In contrast, long-term (~10 years) evaluations on controls were rarely reported (Masiol et al., 2019). The majority of such studies have focused primarily on the changes in concentrations of criterion air pollutants to qualitatively deduce the efficacy of source control (Cheng et al., 2019; Lyu et al., 2017; Li et al., 2020b; Wang et al., 2014). For example, Vu et al. (2019) and Liang et al. (2016) applied random forest and non-parametric methods to normalize the impact of meteorological factors to evaluate the changes in air pollutant concentrations and the effect of control measures in Beijing and other cities in China over recent time periods. However, quantitative evaluations of source emissions have not been common (Gulia et al., 2018), due to the lack of long-term particle composition monitoring (Hopke et al., 2020) and only a handful of studies quantitatively assessing source contributions smoothed the disturbance of weather conditions.

Qingdao, as an economically developed coastal megacity in northern China, has suffered severe air pollution (Bie et al., 2021; Gao et al., 2020; Li et al., 2017). It has been reported by Li et al. (2021a) that meteorology plays a critical role in the formation of pollution for this coastal region. In addition, based on measures taken in accordance with the “CAAP” since 2013 and the “BSPC” since 2018, source interventions such as the relocation and transformation of businesses and industries from the Old Town to port regions (Liu et al., 2021a) have been implemented to improve the air quality in Qingdao. Up to now, the air quality in Qingdao has been greatly improved, the annual mean concentrations of PM_{2.5} and PM₁₀ all decreased by 38% from 2015 to 2020, based on the air quality monitoring data. Liu et al. (2020a) assessed the changes in O₃ concentrations during the Shanghai Cooperation Organization (SCO) Summit in Qingdao and analyzed the impact of control measures on the emissions reduction of its precursors, and Liu et al. (2020b) also analyzed the reasons for the increase of O₃ concentration at nighttime during the SCO Summit. However, there is no report to date has evaluated the effectiveness of these control measures based on a long-term time scale after these control measures were put into practice, especially for quantitating the

设置了格式：非突出显示

设置了格式：下标

设置了格式：下标

设置了格式：非突出显示

设置了格式：非突出显示

changes in source contributions by smoothing the influences of weather conditions. In view of this, our work was mainly to evaluate the implementation of control measures utilizing the data of weather-normalized air pollutants, changes in chemical compositions in PM_{2.5} and source contributions as well as extra source origins from 2011 to 2020. Findings of this work are expected to provide the basis for policy development for a coastal megacity in the future.

2 Materials and methods

2.1 Study region and sampling site

Qingdao is an economically developed coastal megacity of Shandong province, China (Fig. S1). The variation of local economic and social developments from 2011 to 2019 were counted and are shown in Fig. S2. During this period, the local resident population continued to rise, reaching 9499.8 thousand in 2019. The developed area and the possession of civil motor vehicles also showed upward tendency, attaining 758.2 km² and 3062 thousand units in 2019, respectively. The total energy consumption had a maximum of 16891 thousand tons standard coal in 2012 and maintained comparable levels from 2014 to 2019. The industrial coal burning capacity above the designated scale and the volume of liquefied petroleum supply both presented downward trend with values of 10965.7 and 30.2 thousand tons in 2019, respectively. The emissions of sulfur dioxide, nitrogen oxide, and dust basically showed a downward trend from 2011 to 2019, especially in 2017, and the emissions of these pollutants remained at relatively low levels after 2017, reflecting that the pollution sources for these particular pollutants had been effectively controlled in Qingdao.

In this study, in order to evaluate the effectiveness of control measures targeted for polluted sources in the past decade in Qingdao, ambient PM_{2.5} samples were collected at urban sites over three time periods during 2011-2012, 2016, and 2019. The 2011-2012 samples were collected before the “CAAP” was enacted in 2013, and the 2016 samples were collected at the end of the “CAAP”, while the 2019 samples were collected during the middle of the “BSPC” policy period. The sampling plan (detailed in the next section) was designed to capture changes in the data during these periods, as any changes could reflect changes in the pollution sources during different stages of China's air pollution control measures. The sites of Licang and Shinan were sampled in 2011-2012, while five additional sites, Shibei, Laoshan, Chengyang, Huangdao, and Jiaonan were sampled in 2016 and 2019

(Fig. S1). All collection sites were situated on building rooftops ~10–15 m above ground level and used to collect ambient PM_{2.5} samples. Further descriptions of the seven sampling sites are shown in Table S1.

2.2 Sampling and analysis

The sampling periods covered all seasons per year and lasted 41, 56, and 60 days for 2011–2012, 2016, and 2019, respectively (Table S2). Particles were gathered simultaneously to polypropylene filters and quartz filters loaded to sampling instruments. The details of the sampling instruments and filters in the different years are listed in Table S3. Samples were collected for a duration of 22 h from 11:00 to 09:00 of the next day. Field blanks and parallel samples were synchronously collected at each site. Before sampling, to remove some volatile compounds and impurities, the quartz and polypropylene filters were baked in an oven at 500 °C and 60 °C for 2 h, respectively. After sampling, all the filters were stored at 4 °C before gravimetric and chemical analyses were conducted.

Before gravimetric analysis, filter equilibration for 48 h was needed under a constant temperature (20 ± 1 °C) and humidity (45–55%). All filters were weighed by the microbalances with a resolution of 1 or 10 µg during different sampling periods; detailed information is listed in Table S4. To ensure the accuracy, static was eliminated before weighting and all filters were weighed at least twice to meet error requirements (Table S4). For chemical analysis, the elements of Na, Mg, Al, Si, K, Ca, Ti, V, Mn, Fe, Ni, Cu, Zn, and Pb were analyzed in different years. For samples collected in 2011–2012 and 2016, inductively coupled plasma-mass spectrometer (ICP-MS) was applied to determine these elements. For samples collected in 2019, inductively coupled plasma-optical emission spectrometer (ICP-OES) was used to measure all related elements. Water-soluble inorganic ions of NO₃⁻, SO₄²⁻, NH₄⁺, and Cl⁻ were determined using the ion chromatographs during different years. The organic carbon (OC) and elemental carbon (EC) of samples during different years were determined using a thermal/optical carbon analyzer, based on the IMPROVE (in 2011–2012) and IMPROVE_A (in 2016 and 2019) thermal/optical reflectance protocol. The detailed instrumental information is listed in Table S5 and analysis procedures and quality controls are described in Text S1 in the supplemental materials as well as prior works from Liu et al. (2021a), Huang et al. (2021), Wang et al. (2021b), and Tian et al. (2014).

2.3 Random forest (RF) based weather normalization

From 1 January 2015 to 31 December 2020, the hourly concentrations of six air pollutants ($PM_{2.5}$, PM_{10} , SO_2 , NO_2 , CO , and O_3) at the nine national air quality monitoring stations in Qingdao were collected from the China National Environmental Monitoring Network (CNEM) (<http://106.37.208.233:20035>, last access: 29 October 2021). Data collected from the nine monitoring stations were averaged to represent the pollution level at city scale. The explanatory variables including the meteorological variables and time variables were used to build the RF model and predict the air pollutant concentrations. Hourly surface meteorological data including wind speed, wind direction, temperature, dewpoint, relative humidity, and pressure recorded at Qingdao Liuting International Airport were downloaded using the “worldMet” R package (Carslaw, 2017). Time variables included Unix time (number of seconds since 1 January 1970), Gregorian day (day of the year), month, week, weekday, and hour of the day. Data were analyzed in RStudio with a series of packages, and the details of the random forest (RF) model and weather normalization using the RF model are provided in Vu et al. (2019). The training data set was comprised of 80% of the whole data, with the rest as testing data. After the RF predictive model was built for every pollutant, the model was then fed with a new dataset comprised of time variables same with the original dataset and meteorological variables that resampled from the whole observation. The prediction process was repeated 500 times to predict the concentration of a pollutant. The 500 predicted concentrations were then averaged to calculate the weather normalized concentration. The RF based weather normalization technique has been extensively used to decouple meteorology from the observed concentrations, thus can detect interventions in emissions over time (Dai et al., 2020; Grange et al., 2018; Grange and Carslaw, 2019; Hou et al., 2022).

2.4 Theil-Sen regression

The Theil-Sen regression technique has been commonly used to explore the long-term trend of pollutants over years. This approach assumes monotonic linear trends (Masiol et al., 2019). Its principle is to calculate the slopes of all possible pairs of pollutant concentrations, select the median value, and give accurate confidence intervals (Munir et al., 2013; Sen, 1968). In this study, the data of air pollutants obtained from RF modelling with weather

200 normalization was de-seasonalized as the Theil-Sen regression being performed. The Theil-
201 Sen function is provided by the “openair” R package.

202 2.5 Dispersion normalization

203 Although the RF-based weather normalization method can well decouple the overall
204 weather effects, it needs a large size of data to well training the model before de-weathering.
205 The fact that there is a big difference in the size and time-resolution between the routine air
206 quality data and the offline filter-based measured PM_{2.5} chemical compositional data.
207 However, the meteorological dispersion can be quantified by the ventilation coefficient (VC)
208 (Kleinman et al., 1976; Iyer and Raj, 2013). Although the VC-normalization that needs VC
209 data to be known a priori can only decouple the local dispersion, it is relatively simple and
210 useful to decouple the impact of dispersion (Ding et al., 2021). Therefore, this normalized
211 approach is very suitable for the offline data with small size and poor continuity.

212 In this study, the ~~The concentrations of ambient particles are affected by both local~~
213 ~~emissions and meteorological dispersion (Sujatha et al., 2016). Dispersion normalization~~
214 ~~helps stabilize the variation of concentrations due to atmospheric dispersion (Sofowote et al.,~~
215 ~~2021); therefore, in this study, the contributions of local emissions to particle concentrations~~
216 ~~were highlighted. Research suggests that the quantities for particles dispersion can be~~
217 ~~determined by the ventilation coefficient (VC) (Kleinman et al., 1976; Iyer and Raj, 2013);~~
218 VC which data is defined as obtained from the multiplication of mixed layer height (MLH)
219 and the mean wind speed (WS) within the mixed layer (Eq. (1)). Basing on a VC at a given
220 time interval i , the normalized concentration can be obtained by Eq. (2):

$$221 \quad VC_i = MLH_i \times WS_i \quad (1)$$

$$222 \quad C_{vc,i} = C_i \times \frac{VC_i}{VC_{mean}} \quad (2)$$

223 where VC_i ($\text{m}^2 \text{s}^{-1}$) is the ventilation coefficient during period i , VC_{mean} ($\text{m}^2 \text{s}^{-1}$) is the mean
224 VC during the whole study period, and $C_{vc,i}$ ($\mu\text{g m}^{-3}$) and C_i ($\mu\text{g m}^{-3}$) are the normalized and
225 observed concentrations, respectively. In this study, the dispersion normalization was
226 conducted for the data of offline PM_{2.5} and chemical compositions and the resolved source
227 contributions. The surface wind speed at 10 m was replaced with the mean wind speed
228 through MLH because of the absence of wind speed at different heights (Dai et al., 2020;

设置了格式：非突出显示

设置了格式：非突出显示

设置了格式：下标

设置了格式：非突出显示

设置了格式：非突出显示

设置了格式：非突出显示

设置了格式：非突出显示

设置了格式：非突出显示

设置了格式：非突出显示

设置了格式：非突出显示

设置了格式：非突出显示

设置了格式：非突出显示

设置了格式：非突出显示

Ding et al., 2021). The 3 h resolution data of MLH and WS was derived from archived meteorology of the National Ocean and Atmospheric Administration (<https://www.ready.noaa.gov/READYamet.php>, last access: 29 October 2021), and the calculated daily MLH and WS data were used in this study.

2.6 Positive matrix factorization (PMF)

In order to assess the effectiveness of pollution control, source categories and their contributions were estimated by the PMF method. The PMF decomposes a sample composition dataset (X) into two matrices including source profiles (F) and source contributions (G) (Paatero and Tapper, 1994). This principle can be refined as follows:

$$x_{ij} = \sum_{k=1}^p g_{ik} f_{kj} + e_{ij} \quad (3)$$

where x_{ij} is the concentration ($\mu\text{g m}^{-3}$) of the j th component from the i th sample; g_{ik} means the contribution ($\mu\text{g m}^{-3}$) of the k th source to the i th sample; f_{kj} represents the source profile ($\mu\text{g m}^{-3}$) of the j th component from the k th source; e_{ij} is the residual ($\mu\text{g m}^{-3}$) of the j th component of the i th sample; and p means the number of sources. In this study, US EPA PMF v5.0 was applied to carry out source apportionment, and the details in treatment of input data and method detection limits of chemical compositions are described in Table S6 and Text S2, respectively. Bootstrap (BS) and displacement (DISP) analyses were used to investigate the effects of measurement error and rotation ambiguity on the resulting solutions.

2.7 Potential source contribution function (PSCF)

We performed PSCF to further investigate the origin of polluted sources. First, the 72 h backward trajectories were calculated at 6 h intervals every day with starting height of 100 m above ground level in Qingdao (36.10° N, 120.32° E), using the Hybrid Single-Particle Lagrangian Integrated Trajectory (HYSPLIT) model in the GIS-based software of TrajStat (Wang et al., 2009). The weather data was acquired from Global Data Assimilation System with horizontal resolution of one-degree latitude-longitude (available at <http://www.arl.noaa.gov/>, last access: 29 October 2021). PSCF was then analyzed based on the trajectories added to source concentrations. The study region was divided into equal-sized grid cells, thus the number of endpoints for given specific values in every cell could be obtained. According to pre-set threshold criterion, the PSCF value was the proportion of the

number of endpoints beyond the threshold criterion in each cell. To improve the accuracy of the result, weighted PSCF was calculated. More details are given in Text S3 of supplementary material.

3 Results and discussion

3.1 Variation characteristics of the air quality

3.1.1 Trend analysis and annual changes

The annual mean concentration of $PM_{2.5}$ and PM_{10} in Qingdao decreased by 38% and 38% from 51 and 98 $\mu g m^{-3}$ in 2015 to 32 and 61 $\mu g m^{-3}$ in 2020, respectively. The annual mean $PM_{2.5}/PM_{10}$ was 0.47 ± 0.02 , with little change from 2015 to 2020, suggesting the significant impact of coarse particle sources (e.g. dust) in Qingdao. The annual mean levels of SO_2 and NO_2 declined by 72% and 8% from 27 and 33 $\mu g m^{-3}$ in 2015 to 8 and 31 $\mu g m^{-3}$ in 2020, respectively. The concentration of SO_2 showed a significant downward trend, while that of NO_2 changed little, probably indicating that the impact of coal-fired sources was significantly reduced, while the impact of mobile sources might still be obvious. The annual mean level of CO decreased by 32% from 0.91 $mg m^{-3}$ in 2015 to 0.62 $mg m^{-3}$ in 2020, while that of O_3 changed little with ranging from 71 to 69 $\mu g m^{-3}$.

In order to shield the impact of meteorological dispersion, the normalized air quality parameters were acquired using the RF algorithm under 30-year average (1990–2020) meteorological conditions. The Theil–Sen trends of air pollutant concentrations after weather normalization by RF modelling are shown in Fig. 1. The decreasing real trend for air pollutants except for O_3 was found after the weather normalization (Fig. 1), indicating that the air quality is gradually improving in Qingdao. The trends of the normalized air quality parameters represent the effects of emission control and, in some cases, associated chemical processes (Vu et al., 2019). The Theil-Sen trend analysis of air pollutant concentrations and $PM_{2.5}/PM_{10}$ and SO_2/NO_2 after the weather normalization is shown in Fig. 1. Compared with other air pollutants, the decline rate of SO_2 concentration was the highest (15.5% yr^{-1}), whereas that of O_3 concentration was the lowest (0.2% yr^{-1}). Note that the decline rate of $PM_{2.5}$ concentration (6.0% yr^{-1}) was higher than that of PM_{10} concentration (5.6% yr^{-1}), which led to a slight downward trend for $PM_{2.5}/PM_{10}$ (0.6% yr^{-1}), indicating that the impact of coarse particle sources such as dust might be prominent. The decline rate of SO_2

concentration was higher than that of NO₂ concentration (1.0% yr⁻¹), resulting in a higher SO₂/NO₂ decline rate of 15.3% yr⁻¹, indicating that the control effect of stationary sources was better than that of mobile sources (Nirel and Dayan, 2001). It was found that CO concentration also performed an obvious decreasing trend, with the decreasing rate reaching 5.2% yr⁻¹, whereas the downward trend of O₃ concentration was not prominent. The normalized medians of PM_{2.5}, PM₁₀, SO₂, NO₂, CO and O₃ decreased by 2.8, 5.4, 3.4, 0.3, 42.8, and 0.1 µg m⁻³ yr⁻¹, respectively (Table S7). Similar to this study, Vu et al. (2019) found that primary emission controls required by the CAAP in Beijing have led to substantial reductions in PM_{2.5}, PM₁₀, NO₂, SO₂, and CO from 2013 to 2017 of approximately 34%, 24%, 17%, 68%, and 33%, respectively, after meteorological normalization. Zhai et al. (2019) suggested that the mean PM_{2.5} decreased across China was 4.6 µg m⁻³ yr⁻¹ in the meteorology-corrected data from 2013 to 2018, and the Beijing-Tianjin-Hebei, the Yangtze River Delta, the Pearl River Delta, the Sichuan Basin, and the Fenwei Plain decreased 8.0, 6.3, 2.2, 4.9, and 5.0 µg m⁻³ yr⁻¹, respectively. Overall, the concentrations of most air pollutants (i.e., PM_{2.5}, PM₁₀, SO₂, NO₂, and CO) in China have showed a decreasing trend in recent years (Zhao et al., 2021a; Fan et al., 2020), while that of O₃ has performed an increasing trend (Li et al., 2020a; Ma et al., 2021), which further facilitated secondary particles formation (Wang et al., 2016; Nøjgaard et al., 2012).

Figure S3 compares the trends of air pollutants before and after normalization from 2015 to 2020, which are largely different depending on meteorological conditions (Vu et al., 2019). The annual average concentrations of PM_{2.5}, PM₁₀, SO₂, NO₂, CO, and O₃ after normalization were higher than the actual observed concentrations. Compared with 2018, the observed concentrations of air pollutants in 2019 showed an increase in varying degrees; however, the increasing values of annual average concentrations for PM_{2.5}, PM₁₀, SO₂, CO, and O₃ after normalization decreased, and even the NO₂ concentration after normalization also decreased. This indicates that the meteorological conditions in 2019 reduced the effect of actual control to some extent. Up to that point, emission control had resulted in reductions of PM_{2.5}, PM₁₀, SO₂, NO₂, CO, and O₃ concentrations by 17.7%, 31.9%, 18.4%, 1.7%, 0.3%, and 0.4% from 2015 to 2020, respectively, highlighting that much work is still needed to ensure the decrease of NO₂ and O₃ concentrations in the future.

3.1.2 Changes in the air quality in the two control stages

In order to assess the changes in ambient air quality in Qingdao during different policy control periods, this study analyzed the changes in air pollutant concentrations during two stages: the CAAP period (stage 1: 2015-2017) and the BSPC period (stage 2: 2018-2020). The observed annual mean concentrations for PM_{2.5} and PM₁₀ during stage 1 were 45 and 89 $\mu\text{g m}^{-3}$, respectively (Table S8), and their annual average decline rates were 11.9% and 8.0% after weather normalization, respectively. Li et al. (2019b) found that PM_{2.5} decreased by 30-40% across China during 2013-2017 in response to the governmental Clean Air Action. Compared with stage 1, the annual average concentrations of PM_{2.5} and PM₁₀ observed in stage 2 were 35 and 71 $\mu\text{g m}^{-3}$, respectively (Table S8), and the decline range after normalization was reduced, with the decline rates of 5.3% and 7.0%, respectively (Fig. 2). However, PM_{2.5}/PM₁₀ ratios during two stages were less than 0.5, suggesting that the impact of dust sources might be obvious in the two stages. Note that the mean observed annual concentration of SO₂ was 21 $\mu\text{g m}^{-3}$ in the stage 1 (Table S8) and its annual average decline rate reached 25.0% after normalization (Fig. 2), which was significantly higher than that of other pollutants. Compared with stage 1, the observed annual average concentration of SO₂ in stage 2 was only 8 $\mu\text{g m}^{-3}$ (Table S8), and the annual decline rate of SO₂ concentration after normalization still reached 17.1% (Fig. 2), indicating that Qingdao had achieved remarkable results in the control of coal combustion during the two stages. The observed annual mean concentrations for NO₂ and O₃ during stage 1 were 34 and 73 $\mu\text{g m}^{-3}$, respectively (Table S8), and their annual increasing rates after normalization were 1.5% and 2.8%, respectively (Fig. 2). Study showed that surface ozone pollution in China worsened over the stage 1 (Li et al., 2019b). The observed annual mean concentrations of NO₂ and O₃ in stage 2 were 32 and 71 $\mu\text{g m}^{-3}$, respectively (Table S8), while their annual decline rates after normalization were only 2.7% and 2.0%, respectively (Fig. 2). This indicates that the impact of motor vehicles in Qingdao could be greater than expected. Meanwhile, NO₂ and volatile organic compounds emitted from motor vehicles are important precursors for the formation of O₃ (Pugliese et al., 2014; Tsai et al., 2010), which were found to have further enhanced the O₃ concentration in Qingdao's atmosphere. The mean observed annual concentrations for CO were 0.80 and 0.64 mg m^{-3} in stages 1 and 2, respectively (Table S8), and the annual average decline rate were

11.4% and 3.2% after normalization, respectively (Fig. 2), suggesting that there might have been a benefit from the significant control effect of coal-fired sources.

Diurnal variations of concentrations of air pollutants and $PM_{2.5}/PM_{10}$ and SO_2/NO_2 after normalization in the two stages are shown in Fig. S4. The diurnal variation in $PM_{2.5}$ concentration in the two stages was basically the same; however, the concentration of $PM_{2.5}$ in stage 2 was significantly lower than that in stage 1. Diurnal variation of PM_{10} concentration in the two stages was similar to $PM_{2.5}$. The daily variations of $PM_{2.5}/PM_{10}$ in the two stages were basically the same, and the $PM_{2.5}/PM_{10}$ between 06:00-20:00 in stage 2 was slightly lower than that in stage 1, probably suggesting that the impact of dust increased slightly during this period. The diurnal variations of SO_2 and CO concentrations during stages 1 and 2 were generally consistent, whereas their concentrations in stage 2 were substantially lower than those in stage 1, which might indicate that the control effects of coal combustion in Qingdao in stage 2 was obvious. In contrast, the diurnal variations of NO_2 concentrations in stages 1 and 2 were basically consistent with the values at each time, suggesting that the impact of motor vehicles in Qingdao might still be significant, especially the morning and evening peaks and between 21:00 and 23:00 at night. The daily variations of O_3 concentrations were highly consistent in the two stages, especially between 14:00 and 17:00, O_3 pollution was still severe. In general, compared with stage 1, the concentrations of $PM_{2.5}$, PM_{10} , SO_2 , and CO in stage 2 decreased remarkably at all times, while those of NO_2 and O_3 remained basically unchanged at all times, indicating that the control effect of coal-fired sources in Qingdao was significant, whereas the impact of motor vehicles and O_3 pollution were more obvious.

3.1.3 Changes in air quality after the COVID-19 lockdown

In response to the COVID-19 outbreak, a series of lockdown measures were implemented in China to curb the virus transmission, resulting in a significant decrease in traffic and industrial activities. These limitations provided an opportunity to investigate critical pollution sources that could potentially be better managed in the future to further improve the air quality. In order to explore the changes of air quality in Qingdao during the COVID-19 lockdown period, combined with the specific lockdown situation of Qingdao (http://wsjkw.shandong.gov.cn/ywdt/xwtt/202001/t20200124_3420319.html;

378 http://www.shandong.gov.cn/art/2020/3/7/art_119816_350607.html; last access: 29 October
379 2021), this study divided the lockdown period into three stages: pre-lockdown (1 to 24
380 January, 2020), full lockdown (25 January to 7 March, 2020), and partial lockdown (8 to 31
381 March, 2020). The time series and average values of air pollutant concentrations and
382 PM_{2.5}/PM₁₀ and SO₂/NO₂ during different lockdown stages and their corresponding periods
383 in 2018 and 2019 are shown in Fig. 3 and Tables S9-S10. According to the weather
384 normalization data, compared with that before the lockdown, the concentrations of PM_{2.5},
385 PM₁₀, SO₂, NO₂, and CO decreased substantially during the full lockdown, among which the
386 concentrations of PM₁₀ and NO₂ decreased the most (49.5% and 49.0%, respectively),
387 followed by PM_{2.5} (47.8%) (Table S11), which was closely related to the significant decrease
388 in traffic and construction activities during the full lockdown (Collivignarelli et al., 2021;
389 Hong et al., 2021; Wang et al., 2021a). Note that the O₃ concentration increased apparently
390 by 50.8% during the full lockdown (Table S11), suggesting that the atmospheric oxidation
391 might be enhanced during this period, similar to the study of Chu et al. (2021), Ding et al.
392 (2021), He et al. (2020), and Le et al. (2020). Meanwhile, the markedly decrease of NO₂
393 during the full lockdown can also weaken “NO_x titration effect”, further resulting in higher
394 O₃ level during this period. PM₁₀ and NO₂ concentrations rebounded significantly during
395 partial lockdown, increasing by 20.3% and 21.1% compared with the full lockdown,
396 respectively, likely due to the increased impacts of traffic activities and related road dust. The
397 concentrations of PM_{2.5}, SO₂, and CO further decreased during the partial lockdown. The
398 study from Yin et al. (2021) showed that the decrease of PM_{2.5} concentration might be mainly
399 due to the meteorological conditions.

400 Compared with the same period in 2018, the concentrations of PM_{2.5}, PM₁₀, SO₂, NO₂,
401 CO, and O₃ decreased obviously during the full lockdown, of which the reduction range of
402 SO₂ concentration was the greatest (39.8%), whereas that of O₃ concentration was relatively
403 lowest (1.8%) (Table S12). Compared with the corresponding period in 2019, the
404 concentrations of PM_{2.5}, PM₁₀, SO₂, NO₂, and CO decreased by 34.5%, 44.8%, 27.0%, 32.6%,
405 and 22.3% during the full lockdown, respectively, while that of O₃ increased by 3.9% (Table
406 S12). This shows that the COVID-19 lockdown measures led to the marked decrease of the
407 primary emissions of air pollutants. Meanwhile, the concentrations of particulate matter and

设置了格式: 非突出显示

设置了格式: 下标

设置了格式: 非突出显示

设置了格式: 非突出显示

设置了格式: 非突出显示

设置了格式: 下标

NO₂ decreased substantially during the full lockdown. Since there are relatively few industrial enterprises in urban area of Qingdao, NO₂ is mainly emitted from motor-vehicles. Therefore, this suggested that the control of motor-vehicles under normal conditions should play an important role in the improvement of air quality in Qingdao.

3.2 Changes in meteorological conditions and chemical compositions

In this study, the VC in the same period was used to normalize the concentrations of chemical compositions in PM_{2.5}. After decoupling the impacts of meteorological dispersion, the changes in the concentrations of major chemical compositions in the different years were analyzed to better reflect the impacts of source emissions (Dai et al., 2020; Ding et al., 2021). In 2011-2012, 2016, and 2019, the annual average MLHs in Qingdao were 399, 383, and 414 m, respectively (Fig. S5). However, the average wind speed in 2016 was significantly higher than that in other years, reaching 3.3 m s⁻¹. The VC showed an increasing trend year by year, from 1292.7 to 1555.4 m² s⁻¹ (Fig. S5), suggesting that the atmospheric dispersion conditions in Qingdao were gradually increasing. The average VC of Qingdao in three years was 1432.6 m² s⁻¹, and higher MLH usual corresponds to higher wind speed. Time series of observed concentrations and normalized concentrations of PM_{2.5} and chemical compositions are shown in Fig. S6. The observed and VC normalized concentrations of PM_{2.5} during the whole study period were 93 and 83 µg m⁻³, respectively, suggesting that the unfavorable meteorological conditions might increase approximately 10 µg m⁻³ of PM_{2.5}, which was substantially lower than that reported by the study of Ding et al. (2021) in Tianjin. Zhai et al. (2019) found that the mean PM_{2.5} in the meteorology-corrected data from 2013 to 2018 was 12% lower than in the original data, meaning that 12% of the PM_{2.5} decrease in the original data was attributable to the meteorology. However, Gong et al. (2022) suggested that the meteorology can explain approximately 20-33% of the PM_{2.5} variations.

The annual changes in the observed and dispersion normalized concentrations and percentages of main chemical compositions in ambient PM_{2.5} are shown in Fig. 4 and Fig. S7. From 2011-2012 to 2019, the observed concentrations of SO₄²⁻ showed an obvious downward trend, from 23.5 to 6.7 µg m⁻³. The trend of concentrations of SO₄²⁻ after dispersion normalization was consistent with the observed concentrations, and the annual average decline rate was approximately 41.5% (38.1% in 2016 and 44.8% in 2019) (Table S13),

设置了格式: 上标

设置了格式: 上标

probably suggesting that the impacts of coal-fired sources in Qingdao has decreased substantially in recent years. In contrast, the observed concentrations and percentages of NO_3^- increased significantly from 2011-2012 ($3.5 \mu\text{g m}^{-3}$) to 2019 ($10.0 \mu\text{g m}^{-3}$), and $\text{NO}_3^-/\text{SO}_4^{2-}$ increased from 0.14 to 1.50. After dispersion normalization, the concentrations and percentages of NO_3^- changed inappreciable in 2016-2019 but significantly higher than that prior to the CAAP. It has been found that ambient NO_3^- in urban mainly originates from the secondary conversion of NO_x emitted by motor-vehicles (Alexander et al., 2020; Liu et al., 2017; Meng et al., 2008), thereby indicating that the impacts of motor-vehicles in Qingdao might become increasingly obvious. The observed and normalized concentrations and percentages of OC and EC basically performed a downward trend from 2011 to 2019. The OC concentration decreased significantly, and the observed and normalized concentrations decreased from 13.1 to $7.6 \mu\text{g m}^{-3}$ and 12.9 to $7.2 \mu\text{g m}^{-3}$, respectively, which might be related to the significant decrease in the impacts of coal-fired sources in Qingdao. Note that the annual variations of observed and normalized concentrations of NH_4^+ were consistent with that of SO_4^{2-} , but contrary to that of NO_3^- , which might indicate that ammonium mainly existed in the form of ammonium sulfate and ammonia hydrogen sulfate in Qingdao.

Crustal elements (Si, Al, and Mg) decreased remarkably after the CAAP were in place. The observed and normalized concentrations of these elements in 2011-2012 were higher than those in 2016 and 2019, while their concentrations in 2019 were slightly higher than those in 2016. From 2011-2012 to 2019, the observed concentrations of Si, Al, and Mg decreased from 10.7 to $1.0 \mu\text{g m}^{-3}$, 3.1 to $0.5 \mu\text{g m}^{-3}$, and 1.9 to $0.2 \mu\text{g m}^{-3}$, respectively, and the trends of normalized concentrations were consistent with the observed concentrations, likely suggesting that the impact of dust in 2011-2012 was apparently higher than that in 2016 and 2019, and 2019 rebounded compared with 2016. The trends of the observed and normalized concentrations and percentages of Ca were consistent. The concentrations and percentages in 2011-2012 were remarkably higher than that in 2016 and 2019, and the concentration in 2019 rebounds compared with that in 2016, with the increasing rate of 77.1% in terms of normalized data (Table S13). This suggests that the impact of construction activities in 2011-2012 might have been significantly higher than that in 2016 or 2019. The annual trends of observed and normalized concentrations of Fe were also consistent. The

observed and normalized concentrations in 2011-2012 were 4.0 and 4.6 $\mu\text{g m}^{-3}$, respectively. After 2016, the concentrations and percentages of Fe decreased substantially, which might be closely related to the relocation of iron and steel enterprises in Qingdao (Liu et al., 2021a). The observed and normalized concentrations and percentages of Ni and V basically showed a downward trend from 2011-2012 to 2019. The concentrations in 2011-2012 were significantly higher than that in 2016 and 2019, which might indicate that the impact from ships in 2011-2012 was more obvious. Of course, it might also be related to the impact of manual dust sources. From 2011-2012 to 2019, the observed and normalized concentrations and percentages of Na showed a downward trend. The concentration and percentage in 2011-2012 were significantly higher than those in 2016 and 2019, suggesting that the impact of sea salt might have decreased in Qingdao in recent years.

3.3 Changes in source contributions

3.3.1 Source identification

Given that the differences of source profiles during different periods, PMF analysis was conducted for three data sets corresponding to separate sampling periods (i.e., 2011-2012, 2016, and 2019). The solutions from five to nine factors were examined in terms of scaled residuals, factor interpretability, and displacement acceptability (Brown et al., 2015; Dai et al., 2020). An eight-factor solution was chosen as the optimal fits for each data set. The correlation coefficients (R^2) between the observed and calculated concentrations were 0.91, 0.83, and 0.91, respectively (Fig. S8). There were no DISP swaps, and all BS runs had at least 87% agreement with the base case values (Table S14).

The factor profiles estimated from PMF during different periods are shown in Figs. S9-S11. The first factor was identified as vehicle emissions, because OC and EC both had high concentrations and explained variations as well as narrow DISP bounds. It is known that the OC and EC are important tracers for vehicle emissions (Bi et al., 2019; Gao et al., 2016; Ryou et al., 2018; Xu et al., 2019a). The second factor was characterized by higher concentration and explained variation of Si, and high Al concentrations, and they all had narrow DISP ranges. Si and Al were the indicators for fugitive dust (Begum et al., 2011; Jain et al., 2018; Zhao et al., 2021b). The third factor featured relatively high concentrations and explained variations of OC, SO_4^{2-} , and Cl^- with tight DISP intervals. These species were

distinctive tracers for coal combustion (Huang et al., 2017; Song et al., 2021; Tao et al., 2014).

The fourth factor was characterized by high explained variations of Fe and Mn, and relatively high concentrations of Cu and Zn. Tsai et al. (2020) found that Fe and Mn were related to basic oxygen, iron ore sintering and steel oxidation refining. Querol et al. (2007) and Kuo et al. (2007) have reported that Cu and Zn were released from multiple metal smelting. Therefore, this factor was identified as steel-related smelting. The fifth factor was dominated by high concentrations and explained variations of NO_3^- and NH_4^+ with small DISP bounds, which was identified as secondary nitrate (Esmaeilirad et al., 2020). It was found that SO_4^{2-} and NH_4^+ presented the highest explained variations and concentrations with narrow DISP bounds in the sixth factor. Therefore, this factor was assigned as secondary sulphate (Bove et al., 2016; Jain et al., 2020). The seventh factor was featured by high concentration and explained variation of Ca with a small DISP bound, which was identified as construction dust (Liu et al., 2016; Zhang et al., 2005). The final factor was characterized by highly explained variations of Na, Ni, and V with narrow DISP intervals. In addition, the concentrations of Mg, NO_3^- , SO_4^{2-} , and Cl^- in this factor were also relatively high. Zhang et al. (2021), Liu et al. (2018b), Choi et al. (2013), and Police et al. (2016) have found that sea salt involves high amounts of Na, Mg, NO_3^- , SO_4^{2-} , and Cl^- . Meanwhile, Ni and V are the markers of ship emissions (Manousakas et al., 2017; Zong et al., 2018; Xu et al., 2018). Therefore, this factor was recognized as a mixed source of sea salt and ship emissions.

3.3.2 Change in source contributions

The source apportionment results of ambient $\text{PM}_{2.5}$ in Qingdao from 2011-2012 to 2019 are shown in Fig. 5 and Figs. S12-S15. For vehicle emissions, its contribution showed an increasing trend with each year, from $12.1 \mu\text{g m}^{-3}$ (7.9%) to $13.6 \mu\text{g m}^{-3}$ (22.5%). The contribution of coal combustion performed a significant downward trend, from $21.3 \mu\text{g m}^{-3}$ (13.9%) in 2011-2012 to $4.5 \mu\text{g m}^{-3}$ (7.5%) in 2019. The contribution of fugitive dust in 2011-2012 was up to $35.3 \mu\text{g m}^{-3}$ (23.1%), significantly higher than $8.5 \mu\text{g m}^{-3}$ (13.2%) in 2016 and $10.2 \mu\text{g m}^{-3}$ (16.8%) in 2019, and the contribution in 2019 rebounded compared with 2016. The contribution of construction dust showed a downward trend year after year, from $14.2 \mu\text{g m}^{-3}$ (9.3%) in 2011-2012 to $2.4 \mu\text{g m}^{-3}$ (4.0%) in 2019. The contribution of steel-related smelting also showed a downward trend year by year, from $15.9 \mu\text{g m}^{-3}$ (10.4%) in 2011-

2012 to $3.0 \mu\text{g m}^{-3}$ (4.9%) in 2019. The significant decline in the impact of steel-related smelting after 2016 might be closely related to the relocation of iron and steel enterprises in Qingdao (Liu et al., 2021a). The contribution of secondary nitrate basically performed a significant upward trend, increasing from $14.5 \mu\text{g m}^{-3}$ (9.5%) in 2011-2012 to $15.2 \mu\text{g m}^{-3}$ (25.2%) in 2019, which might be related to the high concentration of precursor (NO_2) (Fig. 1) and the increase in atmospheric oxidation in recent years (Chen et al., 2020c; Fu et al., 2020). In contrast, the contribution of secondary sulphate showed a significant downward trend, from $34.2 \mu\text{g m}^{-3}$ (22.3%) in 2011-2012 to $9.7 \mu\text{g m}^{-3}$ (16.0%) in 2019, likely due to the significant decrease in the concentration of its precursor (SO_2) (Fig. 1). For sea salt and ship emissions, the contribution basically performed a downward trend, from $5.7 \mu\text{g m}^{-3}$ (3.7%) in 2011-2012 to $2.0 \mu\text{g m}^{-3}$ (3.2%) in 2019.

To shield the impact of meteorology on the source apportionment results, this study used Eq. (2) to conduct the treatment of dispersion normalization for the source apportionment results, and then analyzed the annual changes in the contributions of different source categories, as shown in Fig. S16. The annual changes in the contributions of multiple sources in Qingdao were basically consistent with the results of direct PMF calculation. The contribution of vehicle emissions was increasing year by year, and the annual average increase rate of contribution concentration was 12.1%. However, the contribution of coal combustion showed a continuous yearly downward trend, with the average annual decline rate of contribution concentration being 56.8%. For fugitive dust, compared with 2011-2012, the contribution in 2016 decreased substantially, with a decline rate of contribution concentration of 68.9%, while it rebounded in 2019, with an increase rate of 25.2%. The contribution of construction dust performed a continuous yearly downward trend, with the average annual decline rate of contribution concentration being 55.9%. For the steel-related smelting, and sea salt and ship emissions, the average annual decline rates of their contribution concentrations were 55.3% and 46.0%, respectively. In contrast, the contribution of secondary nitrate showed an increasing trend, and the increase rate of its contribution concentration was 1.7%, while the contribution proportion increased by more than 70%. The contribution of secondary sulphate showed a continuous yearly downward trend, and the average annual decline rate of contribution concentration was 38.7%. Overall, the impacts of

558 coal combustion and steel-related smelting industrial sources in Qingdao decreased
559 substantially over the last decade, suggesting that the controlling effects of these sources were
560 obvious. The impact of motor-vehicles was prominent each year. Qingdao also risks increased
561 emissions from the increased vehicular population and ozone pollution that facilitate
562 secondary particles formation in the future. The impact of fugitive dust had decreased in
563 recent years, whereas its contribution was still obvious. Therefore, the control of motor-
564 vehicles and dust should be the focus of pollution source control in Qingdao in the future,
565 while that of coal combustion and industrial sources also should not be ignored.

设置了格式: 字体: 非加粗

566 Furthermore, with the beginning of heating season in northern cities in China (Liu et
567 al., 2016; Li et al., 2019a), the atmospheric pollutant emissions increased substantially (Chen
568 et al., 2020a). Coupled with the adverse meteorological conditions (Li et al., 2019a), haze
569 episodes occurred frequently during this period (Liu et al., 2018a; Yang et al., 2020).
570 Therefore, the control effects of pollution sources and key control sources in the specific
571 period can be better highlighted through analyzing the changes in the contributions of
572 emission sources during heating seasons over the years. In this study, the heating season in
573 2011-2012 was defined from 15 to 29 February, 2012, that in 2016 was defined from 17 to 20
574 December, 2016, and that in 2019 referred from 12 to 26 January, 2019. The contributions of
575 different sources during different heating seasons in Qingdao are shown in Figs. S17-S18.
576 Compared with the heating season in 2011-2012, the contribution of coal combustion
577 decreased significantly in the heating seasons of 2016 and 2019, from $50.2 \mu\text{g m}^{-3}$ (31.7%) to
578 $10.9 \mu\text{g m}^{-3}$ (6.4%) and $10.6 \mu\text{g m}^{-3}$ (10.8%). The contribution percentages after dispersion
579 normalization showed a consistent trend. For vehicle emissions, the contribution percentages
580 in the heating season increased continuously each year, from 3.9% in 2011-2012 to 22.3% in
581 2019. The results after normalization had the same trend, suggesting that the impact of motor
582 vehicles in heating season was gradually prominent. The contribution of fugitive dust in the
583 heating season in 2011-2012 ($14.2 \mu\text{g m}^{-3}$) was substantially higher than that in 2016 ($3.9 \mu\text{g}$
584 m^{-3}) and 2019 ($12.0 \mu\text{g m}^{-3}$). The contribution in the heating season in 2019 rebounded
585 remarkably compared with that in 2016, and the results of dispersion normalization were
586 consistent. The contribution of construction dust in the heating season in 2019 was markedly
587 lower than that in 2011-2012 and 2016. The contribution of steel-related smelting in the

heating season showed a continuous yearly downward trend, from $22.6 \mu\text{g m}^{-3}$ in the heating season from 2011-2012 to $4.6 \mu\text{g m}^{-3}$ in 2019. However, its contribution percentage in the heating season in 2019 was higher than that in the heating season in 2016, which was consistent with the normalized results, indicating that the impact of steel-related smelting in the heating season had increased, though the contribution percentage was low. The contribution of secondary nitrate in heating season in 2016 was up to $61.3 \mu\text{g m}^{-3}$ (36.3%), which was significantly higher than that of $28.4 \mu\text{g m}^{-3}$ (28.9%) in 2019 and $16.8 \mu\text{g m}^{-3}$ (10.6%) in 2011-2012. This was consistent with the results of the dispersion normalization. It can be seen that although the contribution of secondary nitrate in the heating season in 2019 was reduced, its contribution was significantly higher than that of other sources. Similarly, the contribution of secondary sulphate was also higher in the heating season of 2016 than other years; however, its contribution was clearly lower than that of secondary nitrate. After dispersion normalization, the contributions of secondary sulphate basically showed a continuous yearly downward trend. The contribution of sea salt and ship emissions in the heating season also showed an obvious downward trend, from $10.0 \mu\text{g m}^{-3}$ (6.3%) in 2011-2012 to $1.4 \mu\text{g m}^{-3}$ (1.5%) in 2019, and the results after dispersion normalization were basically consistent. The average decline rate of contribution concentration was approximately 70%, including 88% in 2016. From this analysis, the impacts of coal combustion and steel-related smelting in Qingdao were relatively low after the heating season in 2016, while that of vehicle emissions was prominent each year. Although the impact of fugitive dust had rebounded in the heating season in 2019, the contribution was relatively low. The contribution of secondary nitrate in heating season was substantially higher than that of other sources, and the influence of secondary sulfate decreased each year. The influence of sea salt and ship emissions in heating season showed a continuous yearly downward trend.

3.4 Changes in potential source areas

Similar to the studies of Liu et al. (2021a) and Dai et al. (2020), according to the source apportionment results, this study used the PSCF method to analyze the changes in the potential impact areas of emission sources in Qingdao from 2011-2012 to 2019, and the results are shown in Fig. 6. For vehicle emissions, the potential impact areas changed greatly from 2011-2012 to 2019. The potential impact areas in 2011-2012 were located at the

618 junction of Shandong, Henan, Anhui, and Jiangsu provinces, and the potential impact areas
619 were mainly located in the south part of Jiangsu in 2016, while in 2019, Tianjin and the
620 northwest part of Shandong were important impact areas. The potential impact areas for
621 fugitive dust showed a trend of westward migration from 2011-2012 to 2019. For 2011-2012,
622 the potential impact areas were located at the junction of Shandong, Henan, Anhui, and
623 Jiangsu, as well as in the northern part of Shandong. The potential impact areas were located
624 in the northwestern part of Shandong in 2016, while they were at the junction of Shandong
625 and Henan in 2019. For coal combustion, the potential impact areas for 2011-2012 were
626 located at the junction of Shandong, Henan, Anhui, and Jiangsu. In 2016, they moved to the
627 northwest of Shandong Province and Beijing Tianjin and Hebei region, and the northwest of
628 Shandong was an important impact area in 2019. For steel-related smelting, Beijing and
629 Tianjin were the potential impact areas for 2011-2012, while the potential impact area was
630 located in the Yellow Sea in 2016, which might be related to the relocation of iron and steel
631 enterprises to a port area in the south of Qingdao (Liu et al., 2021a). This suggests that the air
632 mass transport in the coastal area could lead the nearby sea areas to become potential impact
633 areas. The potential impact area in 2019 was mainly located at the junction of Hebei, Henan,
634 and Shandong.

635 For secondary nitrate, the potential impact area for 2011-2012 was the junction of
636 Shandong, Henan, Jiangsu, and Anhui provinces. The potential impact area was mainly
637 located in the central and southern parts of Shandong in 2016, while two areas were located
638 in Beijing, Tianjin, and the junction of Hebei, Henan, and Shandong provinces in 2019. For
639 secondary sulphate, the main potential impact areas for 2011-2012 were located at the
640 junction of Shandong, Henan, Jiangsu, and Anhui Provinces and the western part of Jilin
641 Province. The impact of the Middle East of Shandong Province was more obvious in 2016,
642 while the impact was greater in the south part of Shandong Province, and the junction of
643 Henan and Jiangsu Provinces in 2019. For construction dust, the main potential impact areas
644 for 2011-2012 were Beijing, Tianjin, and the western part of Shandong Province, and the
645 southeastern part of Hebei Province, Shanghai, and the eastern part of Hubei Province in
646 2016, while the central and western parts of Shandong Province, the junction of Henan and
647 Shandong Provinces, and the central and southern parts of Anhui Province were the main

648 impact areas in 2019. For sea salt and ship emissions, the potential impact areas for 2011-
649 2012 were mainly located in coastal areas of Jiangsu and Shanghai, which were closely
650 related to the impacts of ship emissions from ports and sea salt in these cities. The Yellow Sea
651 was the main impact area in 2016 and 2019, and the impact areas in 2019 moved to the south.
652 Bie et al. (2021) also analyzed the potential impact areas of ship emissions in Qingdao Port
653 from 2018 to 2019 using the PSCF method, and found that they were mainly located in the
654 Bohai Bay, Yellow Sea, and Yangtze River Delta. Overall, from 2011-2012 to 2019, the
655 potential impact areas of different emission sources in Qingdao have changed markedly. In
656 2019, the potential impact areas for most of the emission sources were mainly located in
657 Shandong Province and along the border areas between the western or southwest parts of
658 Shandong and other provinces, while sea salt and ship emissions were mainly affected by
659 transport on the Yellow Sea.

660 **4 Conclusions**

661 A machine learning-based meteorological normalization and a dispersion normalization-
662 based on ventilation coefficient approaches were applied to decouple the meteorological
663 deduced variations in air quality time series and multiple source contributions of a coastal
664 city in northern China (Qingdao), respectively. The concentrations of air pollutants other than
665 ozone in Qingdao decreased substantially and the air quality improved continuously after the
666 “CAAP” period, indicating that the control strategies of air pollution in Qingdao over the
667 years have been proper. The largest emission reduction sections were likely from coal
668 combustions and industrial emissions from 2011-2012 to 2019, and the decrease of steel-
669 related smelting after 2016 due to the relocation of iron and steel enterprises. The
670 contribution of dust in Qingdao decreased remarkably after the “CAAP”, but the impact was
671 still outstanding until 2019. Vehicle emissions were increased in importance, as opposed to
672 the other primary sources. Qingdao risks increased emissions from the increased vehicular
673 population and ozone pollution that facilitate secondary particles formation in the future. In
674 addition, the influence of ship emissions should be gradually reduced. The control of motor-
675 vehicles and dust should be the focus of pollution source control in Qingdao in the future,
676 while that of coal combustion and industrial sources cannot be ignored. In addition, the
677 potential impact areas of different emission sources in Qingdao have changed markedly from

2011-2012 to 2019. The potential impact areas for most of emission sources were mainly located in Shandong and the border areas between western or southwest Shandong and other provinces in 2019, while sea salt and ship emissions were mainly affected from the transport of the Yellow Sea.

Author contributions

Baoshuang Liu: Data curation, Writing – original draft, Yanyang Wang: Data curation and Investigation, He Meng: Data collection, Qili Dai: Supervision and Review, Liuli Diao: Data curation, Jianhui Wu: Supervision, Laiyuan Shi: Supervision, Jing Wang: Supervision, Yufen Zhang: Supervision – review & editing, Yinchang Feng: Supervision – review & editing.

Competing interests

The authors declare no competing financial interests.

Acknowledgements

The authors are grateful to the Qingdao Eco-environment Monitoring Center of Shandong Province for collection of particulate matter samples in this study.

Financial support

This study was financially supported by the National Research Program for Key Issues in Air Pollution Control (No. DQGG2021301), the Tianjin Science and Technology Plan Project (No. PTZWHZ00120) and the Fundamental Research Funds for the Central Universities: Nankai University (No. 63211074).

References

- Alexander, B., Sherwen, T., Holmes, C. D., Fisher, J. A., Chen, Q., Evans, M. J., and Kasibhatla, P.: Global inorganic nitrate production mechanisms: comparison of a global model with nitrate isotope observations, *Atmos. Chem. Phys.*, 20, 3859-3877, <https://doi.org/10.5194/acp-2019-422>, 2020.
- Begum, B. A., Biswas, S. K., and Hopke, P. K.: Key issues in controlling air pollutants in Dhaka, Bangladesh, *Atmos. Environ.*, 45, 7705-7713, <https://doi.org/10.1016/j.atmosenv.2010.10.022>, 2011.
- Beloconi, A., Probst-Hensch, N. M., and Vounatsou, P.: Spatio-temporal modelling of changes in air pollution exposure associated to the COVID-19 lockdown measures across Europe, *Sci. Total Environ.*, 787, 147607, <https://doi.org/10.1016/j.scitotenv.2021.147607>, 2021.
- Bi, X. H., Dai, Q. L., Wu, J. H., Zhang, Q., Zhang, W. H., Luo, R. X., Cheng, Y., Zhang, J. Y., Wang, L., Yu, Z. J., Zhang, Y. F., Tian, Y. Z., and Feng, Y. C.: Characteristics of the main primary source profiles of particulate matter across China from 1987 to 2017, *Atmos. Chem. Phys.*, 19, 3223-3243, <https://doi.org/10.5194/acp-19-3223-2019>, 2019.

712 Bie, S. J., Yang, L. X., Zhang, Y., Huang, Q., Li, J. S., Zhao, T., Zhang, X. F., Wang, P. C., and Wang, W.
713 X.: 2021. Source appointment of PM_{2.5} in Qingdao Port, East of China, *Sci. Total Environ.*, 755,
714 142456, <https://doi.org/10.1016/j.scitotenv.2020.142456>, 2021.

715 Bove, M. C., Brotto, P., Calzolari, G., Cassola, F., Cavalli, F., Fermo, P., Hjorth, J., Massabò, D., Nava,
716 S., Piazzalunga, A., Schembari, C., and Prati, P.: PM₁₀ source apportionment applying PMF and
717 chemical tracer analysis to ship-borne measurements in the Western Mediterranean, *Atmos. Environ.*,
718 125, 140-151, <https://doi.org/10.1016/j.atmosenv.2015.11.009>, 2016.

719 Brown, S. G., Eberly, S., Paatero, P., and Norris, G. A.: Methods for estimating uncertainty in PMF
720 solutions: Examples with ambient air and water quality data and guidance on reporting PMF results,
721 *Sci. Total Environ.*, 518, 626-635, <https://doi.org/10.1016/j.scitotenv.2015.01.022>, 2015.

722 Chen, J. Y., Shan, M., Xia, J. J., and Jiang, Y.: Effects of space heating on the pollutant emission intensities
723 in "2+26" cities, *Building Environ.*, 175, 106817, <https://doi.org/10.1016/j.buildenv.2020.106817>,
724 2020a.

725 Chen, Y., Zhang, S. M., Peng, C., Shi, G. M., Tian, M., Huang, R. J., Guo, D. M., Wang, H. B., Yao, X. J.,
726 Yang, F. M.: Impact of the COVID-19 pandemic and control measures on air quality and aerosol light
727 absorption in Southwestern China, *Sci. Total Environ.*, 749, 141419,
728 <https://doi.org/10.1016/j.scitotenv.2020.141419>, 2020b.

729 Chen, X., Wang, H., Lu, K., Li, C., Zhai, T., Tan, Z., Ma, X., Yang, X., Liu, Y., Chen, S., Dong, H., Li, X.,
730 Wu, Z., Hu, M., Zeng, L., and Zhang, Y.: Field Determination of Nitrate Formation Pathway in Winter
731 Beijing, *Environ. Sci. Technol.*, 54, 9243-9253, <https://doi.org/10.1021/acs.est.0c00972>, 2020c.

732 Cheng, N. L., Cheng, B. F., Li, S. S., and Ning, T. Z.: Effects of meteorology and emission reduction
733 measures on air pollution in Beijing during heating seasons, *Atmos. Pollut. Res.*, 10, 971-979,
734 <https://doi.org/10.1016/j.apr.2019.01.005>, 2019.

735 Choi, J. -K., Heo, J. -B., Ban, S. -J., Yi, S. -M., and Zoh, K. -D.: Source apportionment of PM_{2.5} at the
736 coastal area in Korea, *Sci. Total Environ.*, 447, 370-380,
737 <https://doi.org/10.1016/j.scitotenv.2012.12.047>, 2013.

738 Collivignarelli, M. C., De Rose, C., Abbà, A., Baldi, M., Bertanza, G., Pedrazzani, R., Sorlini, S., and
739 Carnevale Miino, M.: Analysis of lockdown for COVID-19 impact on NO₂ in London, Milan and
740 Paris: What lesson can be learnt? *Process Saf. Environ. Prot.*, 146, 952-960
741 <https://doi.org/10.1016/j.psep.2020.12.029>, 2021.

742 Chu, B. W., Zhang, S. P., Liu, J., Ma, Q. X., and He, H.: Significant concurrent decrease in PM_{2.5} and NO₂
743 concentrations in China during COVID-19 epidemic, *J. Environ. Sci.*, 99, 346-353,
744 <https://doi.org/10.1016/j.jes.2020.06.031>, 2021.

745 Carslaw, D. C.: Worldmet: Import Surface Meteorological Data from NOAA Integrated Surface Database
746 (ISD), available at: <http://github.com/davidcarslaw/> (last access: 5 September 2018), 2017.

747 Cohen, A. J., Brauer, M., Burnett, R., Anderson, H. R., Frostad, J., Estep, K., Balakrishnan, K., Brunekreef,
748 B., Dandona, L., Dandona, R., Feigin, V., Freedman, G., Hubbell, B., Jobling, A., Kan, H., Knibbs,
749 L., Liu, Y., Martin, R., Morawska, L., Pope, C. A., Shin, H., Straif, K., Shaddick, G., Thomas, M., van
750 Dingenen, R., van Donkelaar, A., Vos, T., Murray, C. J. L., and Forouzanfar, M. H.: Estimates and 25-
751 year trends of the global burden of disease attributable to ambient air pollution: an analysis of data
752 from the Global Burden of Diseases Study 2015, *The Lancet.*, 389, 1907-1918,
753 [https://doi.org/10.1016/S0140-6736\(17\)30505-6](https://doi.org/10.1016/S0140-6736(17)30505-6), 2017.

754 Cucciniello, R., Raia, L., and Vasca, E.: Air quality evaluation during COVID-19 in Southern Italy: the
755 case study of Avellino city, *Environ. Res.*, 203, 111803, <https://doi.org/10.1016/j.envres.2021.111803>,

2022.

Dai, Q. L., Liu, B. S., Bi, X. H., Wu, J. H., Liang, D. N., Zhang, Y. F., Feng, Y. C., and Hopke, P. K.: Dispersion Normalized PMF Provides Insights into the Significant Changes in Source Contributions to PM_{2.5} after the COVID-19 Outbreak, *Environ. Sci. Technol.*, 54, 9917-9927, <https://doi.org/10.1021/acs.est.0c02776>, 2020.

Dai, Q. L., Ding, J., Hou, L. L., Li, L. X., Cai, Z. Y., Liu, B. S., Song, C. B., Bi, X. H., Wu, J. H., Zhang, Y. F., Feng, Y. C., and Hopke, P. K.: Haze episodes before and during the COVID-19 shutdown in Tianjin, China: Contribution of fireworks and residential burning, *Environ. Pollut.*, 286, 117252, <https://doi.org/10.1016/j.envpol.2021.117252>, 2021.

Esmailirad, S., Lai, A., Abbaszade, G., Schnelle-Kreis, J., Zimmermann, R., Uzu, G., Daellenbach, K., Canonaco, F., Hassankhani, H., Arhami, M., Baltensperger, U., Prévôt, A. S. H., Schauer, J. J., Jaffrezo, J. -L., Hosseini, V., and El Haddad, I.: Source apportionment of fine particulate matter in a Middle Eastern Metropolis, Tehran-Iran, using PMF with organic and inorganic markers, *Sci. Total Environ.*, 705, 135330, <https://doi.org/10.1016/j.scitotenv.2019.135330>, 2020.

Fan, H., Zhao, C. F., and Yang, Y. K.: A comprehensive analysis of the spatio-temporal variation of urban air pollution in China during 2014–2018, *Atmos. Environ.*, 220, 117066, <https://doi.org/10.1016/j.atmosenv.2019.117066>, 2020.

Fu, X., Wang, T., Gao, J., Wang, P., Liu, Y. M., Wang, S. X., Zhao, B., and Xue, L. K.: Persistent Heavy Winter Nitrate Pollution Driven by Increased Photochemical Oxidants in Northern China, *Environ. Sci. Technol.*, 54, 3881–3889, <https://doi.org/10.1021/acs.est.9b07248>, 2020.

Gao, J., Peng, X., Chen, G., Xu, J., Shi, G. L., Zhang, Y. C., and Feng, Y. C.: Insights into the chemical characterization and sources of PM_{2.5} in Beijing at a 1-h time resolution, *Sci. Total Environ.*, 542, 162–171, <https://doi.org/10.1016/j.scitotenv.2015.10.082>, 2016.

Gao, Y., Shan, H. Y., Zhang, S. Q., Sheng, L. F., Li, J. P., Zhang, J. X., Ma, M. C., Meng, H., Luo, K., Gao, H. W., and Yao, X. H.: Characteristics and sources of PM_{2.5} with focus on two severe pollution events in a coastal city of Qingdao, China, *Chemosphere*, 247, 125861, <https://doi.org/10.1016/j.chemosphere.2020.125861>, 2020.

Grange, S. K., Carslaw, D. C., Lewis, A. C., Boleti, E., and Hueglin, C.: Random forest meteorological normalization models for Swiss PM₁₀ trend analysis, *Atmos. Chem. Phys.*, 18, 6223–6239, <https://doi.org/10.5194/acp-18-6223-2018>, 2018.

Grange, S. K., and Carslaw, D. C.: Using meteorological normalization to detect interventions in air quality time series, *Sci. Total Environ.*, 653, 578–588, <https://doi.org/10.1016/j.scitotenv.2018.10.344>, 2019.

Gong, S. L., Zhang, L., Liu, C., Lu, S. H., Pan, W. J., and Zhang, Y. H.: Multi-scale analysis of the impacts of meteorology and emissions on PM_{2.5} and O₃ trends at various regions in China from 2013 to 2020 2. Key weather elements and emissions, *Sci. Total Environ.*, 824, 153847, <https://doi.org/10.1016/j.scitotenv.2022.153847>, 2022.

Gulia, S., Mittal, A., and Khare, M.: Quantitative evaluation of source interventions for urban air quality improvement - A case study of Delhi city, *Atmos. Pollut. Res.*, 9, 577-583, <https://doi.org/10.1016/j.apr.2017.12.003>, 2018.

He, G. J., Pan, Y. H., and Tanaka, T.: The short-term impacts of COVID-19 lockdown on urban air pollution in China, *Nat. Sustainability*, 3, 1005-1011, <https://doi.org/10.1038/s41893-020-0581-y>, 2020.

Huang, H. Y., Liu, B. S., Li, S., Choe, T. -H., Dai, Q. L., Gu, Y., Diao, L. L., Zhang, S. F., Bi, X. H., Luo, Z.

W., Lu, M. M., Zhang, Y. F., and Feng, Y. C.: An estimation method for regional transport contributions from emission sources based on a high-mountain site: a case study in Zhumadian, China, *Atmos. Environ.*, 263, 118664, <https://doi.org/10.1016/j.atmosenv.2021.118664>, 2021.

Huang, J., Pan, X. C., Guo, X. B., and Li, G. X.: 2018. Health impact of China's Air Pollution Prevention and Control Action Plan: an analysis of national air quality monitoring and mortality data, *The Lancet Planetary Health.*, 2, e313-e323, [https://doi.org/10.1016/S2542-5196\(18\)30141-4](https://doi.org/10.1016/S2542-5196(18)30141-4), 2018.

Huang, R. J., Zhang, Y. L., Bozzetti, C., Ho, K. F., Cao, J. J., Han, Y. M., Daellenbach, K. R., Slowik, J. G., Platt, S. M., Canonaco, F., Zotter, P., Wolf, R., Pieber, S. M., Bruns, E. A., Crippa, M., Ciarelli, G., Piazzalunga, A., Schwikowski, M., Abbaszade, G., Schnelle-Kreis, J., Zimmermann, R., An, Z. S., Szidat, S., Baltensperger, U., El Haddad, I., and Prevot, A. S. H.: High secondary aerosol contribution to particulate pollution during haze events in China, *Nature*, 514, 218-222, <https://doi.org/10.1038/nature13774>, 2014.

Huang, X. J., Liu, Z. R., Liu, J. Y., Hu, B., Wen, T. X., Tang, G. Q., Zhang, J. K., Wu, F. K., Ji, D. S., Wang, L. L., and Wang, Y. S.: Chemical characterization and source identification of PM_{2.5} at multiple sites in the Beijing-Tianjin-Hebei region, China, *Atmos. Chem. Phys.*, 17, 12941-12962, [10.5194/acp-17-12941-2017](https://doi.org/10.5194/acp-17-12941-2017), 2017.

Hopke, P. K., Dai, Q. L., Li, L. X., and Feng, Y. C.: Global review of recent source apportionments for airborne particulate matter, *Sci. Total Environ.*, 740, 140091, <https://doi.org/10.1016/j.scitotenv.2020.140091>, 2020.

Hong, Y. W., Xu, X. B., Liao, D., Zheng, R. H., Ji, X. T., Chen, Y. T., Xu, L. L., Li, M. R., Wang, H., Xiao, H., Choi, S. D., Chen, J. S.: Source apportionment of PM_{2.5} and sulfate formation during the COVID-19 lockdown in a coastal city of southeast China, *Environ. Pollut.*, 286, 117577, <https://doi.org/10.1016/j.envpol.2021.117577>, 2021.

Hou, L. L., Dai, Q. L., Song, C. B., Liu, B. S., Guo, F. Z., Dai, T. J., Li, L. X., Liu, B. S., Bi, X. H., Zhang, Y. F., and Feng, Y. C.: Revealing drivers of haze pollution by explainable machine learning, *Environ. Sci. Technol. Lett.*, 9, 112-119, <https://doi.org/10.1021/acs.estlett.1c00865>, 2022.

Iyer, U. S., and Raj, P. E.: Ventilation coefficient trends in the recent decades over four major Indian metropolitan cities, *J. Earth Syst. Sci.*, 122, 537-549, <https://doi.org/10.1007/s12040-013-0270-6>, 2013.

Jain, S., Sharma, S. K., Mandal, T. K., and Saxena, M.: Source apportionment of PM₁₀ in Delhi, India using PCA/APCS, UNMIX and PMF, *Particuology*, 37, 107-118, <https://doi.org/10.1016/j.partic.2017.05.009>, 2018.

Jain, S., Sharma, S. K., Vijayan, N., and Mandal, T. K.: Seasonal characteristics of aerosols (PM_{2.5} and PM₁₀) and their source apportionment using PMF: A four year study over Delhi, India, *Environ. Pollut.*, 262, 114337, <https://doi.org/10.1016/j.envpol.2020.114337>, 2020.

Jiang, X., Li, G. L., and Fu, W.: Government environmental governance, structural adjustment and air quality: A quasi-natural experiment based on the Three-year Action Plan to Win the Blue Sky Defense War, *J. Environ. Manage.*, 277, 111470, <https://doi.org/10.1016/j.jenvman.2020.111470>, 2021.

Joshi, P., Ghosh, S., Dey, S., Dixit, K., Choudhary, R. K., Salve, H. R., and Balakrishnan, K.: Impact of acute exposure to ambient PM_{2.5} on non-trauma all-cause mortality in the megacity Delhi, *Atmos. Environ.*, 259, 118548, <https://doi.org/10.1016/j.atmosenv.2021.118548>, 2021.

Kleinman, M. T., Kneip, T. J., and Eisenbud, M.: Seasonal patterns of airborne particulate concentrations in New York City, *Atmos. Environ.* (1967), 10, 9-11, [https://doi.org/10.1016/0004-6981\(76\)90252-3](https://doi.org/10.1016/0004-6981(76)90252-3), 1976.

设置了格式：字体：五号

844 Kuo, S. -C., Hsieh, L. -Y., Tsai, C. -H., and Tsai, Y. I.: Characterization of PM_{2.5} fugitive metal in the
845 workplaces and the surrounding environment of a secondary aluminum smelter, *Atmos. Environ.*, 41,
846 6884-6900, <https://doi.org/10.1016/j.atmosenv.2007.04.038>, 2007.

847 Le, T. H., Wang, Y., Liu, L., Yang, J. N., Yung, Y. L., Li, G. H., and Seinfeld, J. H.: Unexpected air
848 pollution with marked emission reductions during the COVID-19 outbreak in China, *Science*, 369,
849 702, <https://doi.org/10.1126/science.abb7431>, 2020.

850 Li, L. Y., Yan, D. Y., Xu, S. H., Huang, M. L., Wang, X. X., and Xie, S. D.: Characteristics and source
851 distribution of air pollution in winter in Qingdao, eastern China. *Environ. Pollut.*, 224, 44-53,
852 <https://doi.org/10.1016/j.envpol.2016.12.037>, 2017.

853 Li, H., You, S. J., Zhang, H., Zheng, W. D., and Zou, L. J.: Analysis of the impacts of heating emissions on
854 the environment and human health in North China, *J. Clean Prod.*, 207, 728-742,
855 <https://doi.org/10.1016/j.jclepro.2018.10.013>, 2019a.

856 Li, K., Jacob, D. J., Liao, H., Zhu, J., Shah, V., Shen, L., Bates, K. H., Zhang, Q., and Zhai, S. X.: A two-
857 pollutant strategy for improving ozone and particulate air quality in China, *Nat. Geosci.*, 12, 906-910,
858 <https://doi.org/10.1038/s41561-019-0464-x>, 2019b.

859 Li, K., Jacob, D. J., Shen, L., Lu, X., De Smedt, I., and Liao, H.: Increases in surface ozone pollution in
860 China from 2013 to 2019: anthropogenic and meteorological influences, *Atmos. Chem. Phys.*, 20,
861 11423-11433, <https://doi.org/10.5194/acp-20-11423-2020>, 2020a.

862 Li, W. J., Shao, L. Y., Wang, W. H., Li, H., Wang, X. M., Li, Y. W., Li, W. J., Jones, T., and Zhang, D. Z.:
863 Air quality improvement in response to intensified control strategies in Beijing during 2013–2019, *Sci.*
864 *Total Environ.*, 744, 140776, <https://doi.org/10.1016/j.scitotenv.2020.140776>, 2020b.

865 Li, Y., Miao, Y. C., Che, H. Z., and Liu, S. H.: On the heavy aerosol pollution and its meteorological
866 dependence in Shandong province, China, *Atmos. Res.*, 256, 105572,
867 <https://doi.org/10.1016/j.atmosres.2021.105572>, 2021a.

868 Li, Y., Xu, H. X., Tang, K. Y., Lau, A. K. H., Fung, J. C. H., and Zhang, X. G.: An ensemble assessment of
869 the effectiveness of vehicular emission control programs for air quality improvement in Hong Kong,
870 *Atmos. Environ.*, 262, 118571, <https://doi.org/10.1016/j.atmosenv.2021.118571>, 2021b.

871 Liang, X., Li, S., Zhang, S. Y., Huang, H., and Chen, S. X.: PM_{2.5} data reliability, consistency, and air
872 quality assessment in five Chinese cities, *J. Geophys. Res. -Atmos.*, 121, 10220-10236,
873 10.1002/2016JD024877, 2016.

874 Liu, B. S., Song, N., Dai, Q. L., Mei, R. B., Sui, B. H., Bi, X. H., and Feng, Y. C.: Chemical composition
875 and source apportionment of ambient PM_{2.5} during the non-heating period in Taian, China, *Atmos.*
876 *Res.*, 170, 23-33, <https://doi.org/10.1016/j.atmosres.2015.11.002>, 2016.

877 Liu, B. S., Cheng, Y., Zhou, M., Liang, D. N., Dai, Q. L., Wang, L., Jin, W., Zhang, L. Z., Ren, Y. B., Zhou,
878 J. B., Dai, C. L., Xu, J., Wang, J., Feng, Y. C., and Zhang, Y. F.: Effectiveness evaluation of temporary
879 emission control action in 2016 in winter in Shijiazhuang, China, *Atmos. Chem. Phys.*, 18, 7019-7039,
880 <https://doi.org/10.5194/acp-18-7019-2018>, 2018a.

881 Liu, B. S., Wu, J. H., Wang, J., Shi, L. Y., Meng, H., Dai, Q. L., Wang, J., Song, C. B., Zhang, Y. F., Feng, Y.
882 C., and Hopke, P. K.: Chemical characteristics and sources of ambient PM_{2.5} in a harbor area:
883 Quantification of health risks to workers from source-specific selected toxic elements, *Environ. Pollut.*,
884 268, 115926, <https://doi.org/10.1016/j.envpol.2020.115926>, 2021a.

885 Liu, C., Xu, R., Zhang, T. H., Zhang, H. D., Zhang, B. H., Cong, C. H., and Wu, J. Y.: Analysis of Ozone
886 Pollution Characteristics and Its Sources During the Shanghai Cooperation Organization Summit in
887 Qingdao, *Meteor. Environ. Sci. (in Chinese)*, 43, 51-58, [28](https://doi.org/10.16765/j.cnki.1673-</p>
</div>
<div data-bbox=)

7148.2020.03.007, 2020a.

Liu, C., Zhang, H. D., Zhang, T. H., Xu, R., Zhang, B. H., Lu, M. Y., and Li, G. H.: The causes of ozone concentration growth in the night during the “Shanghai Cooperation Organization Summit” in Qingdao, China Environ. Sci. (in Chinese), 40, 3332-3341, <https://doi.org/10.19674/j.cnki.issn1000-6923.2020.0372>, 2020b.

Liu, M., Saari, R. K., Zhou, G. X., Li, J., Han, L., and Liu, X.N.: Recent trends in premature mortality and health disparities attributable to ambient PM_{2.5} exposure in China: 2005–2017, Environ. Pollut., 279, 116882, <https://doi.org/10.1016/j.envpol.2021.116882>, 2021b.

Liu, W. J., Xu, Y. S., Liu, W. X., Liu, Q. Y., Yu, S. Y., Liu, Y., Wang, X., and Tao, S.: Oxidative potential of ambient PM_{2.5} in the coastal cities of the Bohai Sea, northern China: Seasonal variation and source apportionment, Environ. Pollut., 236, 514-528, <https://doi.org/10.1016/j.envpol.2018.01.116>, 2018b.

Liu, F., Beirle, S., Zhang, Q., van der, A. R. J., Zheng, B., Tong, D., and He, K.: NOx emission trends over Chinese cities estimated from OMI observations during 2005 to 2015, Atmos. Chem. Phys., 17, 9261-9275, <https://doi.org/10.5194/acp-17-9261-2017>, 2017.

Lyu, X. P., Zeng, L. W., Guo, H., Simpson, I. J., Ling, Z. H., Wang, Y., Murray, F., Louie, P. K. K., Saunders, S. M., Lam, S. H. M., and Blake, D. R.: Evaluation of the effectiveness of air pollution control measures in Hong Kong, Environ. Pollut., 220, 87-94, <https://doi.org/10.1016/j.envpol.2016.09.025>, 2017.

Ma, X. W., Li, C. D., Dong, X. Y., and Liao, H.: Empirical analysis on the effectiveness of air quality control measures during mega events: Evidence from Beijing, China, J. Clean Prod., 271, 122536, <https://doi.org/10.1016/j.jclepro.2020.122536>, 2020.

Ma, X. D., Huang, J. P., Zhao, T. L., Liu, C., Zhao, K. H., Xing, J., and Xiao, W.: Rapid increase in summer surface ozone over the North China plain during 2013–2019: a side effect of particulate matter reduction control? Atmos. Chem. Phys., 21, 1-16, <https://doi.org/10.5194/acp-21-1-2021>, 2021.

Manousakas, M., Papaefthymiou, H., Diapouli, E., Migliori, A., Karydas, A. G., Bogdanovic-Radovic, I., and Eleftheriadis, K.: Assessment of PM_{2.5} sources and their corresponding level of uncertainty in a coastal urban area using EPA PMF 5.0 enhanced diagnostics, Sci. Total Environ., 574, 155-164, <https://doi.org/10.1016/j.scitotenv.2016.09.047>, 2017.

Masiol, M., Squizzato, S., Rich, D. Q., and Hopke, P. K.: Long-term trends (2005–2016) of source apportioned PM_{2.5} across New York State, Atmos. Environ., 201, 110-120, <https://doi.org/10.1016/j.atmosenv.2018.12.038>, 2019.

Meng, Z. Y., Ding, G. A., Xu, X. B., Xu, X. D., Yu, H. Q., and Wang, S. F.: Vertical distributions of SO₂ and NO₂ in the lower atmosphere in Beijing urban areas, China, Sci. Total Environ., 390, 456-465, <https://doi.org/10.1016/j.scitotenv.2007.10.012>, 2008.

Munir, S., Chen, H. B., and Ropkins, K.: Quantifying temporal trends in ground level ozone concentration in the UK, Sci. Total Environ., 458-460, 217-227, <https://doi.org/10.1016/j.scitotenv.2013.04.045>, 2013.

Nøjgaard, J. K., Nguyen, Q. T., Glasius, M., and Sørensen, L. L.: Nucleation and Aitken mode atmospheric particles in relation to O₃ and NO_x at semirural background in Denmark, Atmos. Environ., 49, 275-283, <https://doi.org/10.1016/j.atmosenv.2011.11.040>, 2012.

Nirel, R., and Dayan, U.: On the Ratio of Sulfur Dioxide to Nitrogen Oxides as an Indicator of Air Pollution Sources, J. Appl. Meteorol., 40, 1209-1222, [https://doi.org/10.1175/1520-0450\(2001\)040<1209:OTROSD>2.0.CO;2](https://doi.org/10.1175/1520-0450(2001)040<1209:OTROSD>2.0.CO;2), 2001.

Paatero, P., and Tapper, U.: Positive matrix factorization: A non-negative factor model with optimal

utilization of error estimates of data values. *Environmetrics*, 5, 111-126,
<https://doi.org/10.1002/env.3170050203>, 1994.

Police, S., Sahu, S. K., and Pandit, G. G.: Chemical characterization of atmospheric particulate matter and their source apportionment at an emerging industrial coastal city, Visakhapatnam, India, *Atmos. Pollut. Res.*, 7, 725-733, <https://doi.org/10.1016/j.apr.2016.03.007>, 2016.

Pugliese, S. C., Murphy, J. G., Geddes, J. A., and Wang, J. M.: The impacts of precursor reduction and meteorology on ground-level ozone in the Greater Toronto Area, *Atmos. Chem. Phys.*, 14, 8197-8207, <https://doi.org/10.5194/acp-14-8197-2014>, 2014.

Qi, L., Zhang, Y. F., Ma, Y. H., Chen, M. D., Ge, X. L., Ma, Y., Zheng, J., Wang, Z., and Li, S. Z.: Source identification of trace elements in the atmosphere during the second Asian Youth Games in Nanjing, China: Influence of control measures on air quality, *Atmos. Pollut. Res.*, 7, 547-556, <https://doi.org/10.1016/j.apr.2016.01.003>, 2016.

Querol, X., Viana, M., Alastuey, A., Amato, F., Moreno, T., Castillo, S., Pey, J., de la Rosa, J., Sánchez de la Campa, A., Artíñano, B., Salvador, P., García Dos Santos, S., Fernández-Patier, R., Moreno-Grau, S., Negral, L., Minguillón, M. C., Monfort, E., Gil, J. I., Inza, A., Ortega, L. A., Santamaría, J. M., and Zabalza, J.: Source origin of trace elements in PM from regional background, urban and industrial sites of Spain, *Atmos. Environ.*, 41, 7219-7231, <https://doi.org/10.1016/j.atmosenv.2007.05.022>, 2007.

Ryou, H. G., Heo, J., and Kim, S. Y.: Source apportionment of PM₁₀ and PM_{2.5} air pollution, and possible impacts of study characteristics in South Korea, *Environ. Pollut.*, 240, 963-972, <https://doi.org/10.1016/j.envpol.2018.03.066>, 2018.

Sen, P. K.: Estimates of the Regression Coefficient Based on Kendall's Tau AU – Sen, Pranab Kumar, J. *Am. Stat. Assoc.*, 63, 1379-1389, <https://doi.org/10.1080/01621459.1968.10480934>, 1968.

Schleicher, N., Norra, S., Chen, Y., Chai, F., and Wang, S.: Efficiency of mitigation measures to reduce particulate air pollution—A case study during the Olympic Summer Games 2008 in Beijing, China, *Sci. Total Environ.*, 427-428, 146-158, <https://doi.org/10.1016/j.scitotenv.2012.04.004>, 2012.

Shi, Z. B., Song, C. B., Liu, B. W., Lu, G. D., Xu, J. S., Vu, T. V., Elliott, R. J. R., Li, W. J., Bloss, W. J., and Harrison, R. M.: Abrupt but smaller than expected changes in surface air quality attributable to COVID-19 lockdowns, *Sci Adv.*, 7, eabd6696, <https://doi.org/10.1126/sciadv.abd6696>, 2021.

Sofowote, U. M., Healy, R. M., Su, Y., Debosz, J., Noble, M., Munoz, A., Jeong, C. H., Wang, J. M., Hilker, N., Evans, G. J., Brook, J. R., Lu, G., and Hopke, P. K.: Sources, variability and parameterizations of intra-city factors obtained from dispersion-normalized multi-time resolution factor analyses of PM_{2.5} in an urban environment, *Sci. Total Environ.*, 761, 143225, <https://doi.org/10.1016/j.scitotenv.2020.143225>, 2021.

Sujatha, P., Mahalakshmi, D. V., Ramiz, A., Rao, P. V. N., and Naidu, C. V.: Ventilation coefficient and boundary layer height impact on urban air quality, *Cogent Environ. Sci.*, 2, 1125284 <https://doi.org/10.1080/23311843.2015.1125284>, 2016.

Tian, Y. Z., Wang, J., Peng, X., Shi, G. L., and Feng, Y. C.: Estimation of the direct and indirect impacts of fireworks on the physicochemical characteristics of atmospheric PM₁₀ and PM_{2.5}, *Atmos. Chem. Phys.*, 14, 9469-9479, <https://doi.org/10.5194/acp-14-9469-2014>, 2014.

Tsai, P. J., Young, L. H., Hwang, B. F., Lin, M. Y., Chen, Y. C., and Hsu, H. T.: Source and health risk apportionment for PM_{2.5} collected in Sha-Lu area, Taiwan, *Atmos. Pollut. Res.*, 11, 851-858, <https://doi.org/10.1016/j.apr.2020.01.013>, 2020.

Tsai, D. H., Wang, J. L., Chuang, K. J., and Chan, C. C.: Traffic-related air pollution and cardiovascular mortality in central Taiwan, *Sci. Total Environ.*, 408, 1818-1823,

976 <https://doi.org/10.1016/j.scitotenv.2010.01.044>, 2010.
 977 Vodonos, A., and Schwartz, J.: Estimation of excess mortality due to long-term exposure to PM_{2.5} in
 978 continental United States using a high-spatiotemporal resolution model, *Environ. Res.*, 196, 110904,
 979 <https://doi.org/10.1016/j.envres.2021.110904>, 2021.
 980 Vu, T. V., Shi, Z. B., Cheng, J., Zhang, Q., He, K. B., Wang, S. X., and Harrison, R. M.: Assessing the
 981 impact of clean air action on air quality trends in Beijing using a machine learning technique, *Atmos.*
 982 *Chem. Phys.*, 19, 11303-11314, <https://doi.org/10.5194/acp-19-11303-2019>, 2019.
 983 Wang, D. F., Zhou, B., Fu, Q. Y., Zhao, Q. B., Zhang, Q., Chen, J. M., Yang, X., Duan, Y. S., and Li, J.:
 984 Intense secondary aerosol formation due to strong atmospheric photochemical reactions in summer:
 985 observations at a rural site in eastern Yangtze River Delta of China, *Sci. Total Environ.*, 571, 1454-
 986 1466, <https://doi.org/10.1016/j.scitotenv.2016.06.212>, 2016.
 987 Wang, H. L., Miao, Q., Shen, L. J., Yang, Q., Wu, Y. Z., and Wei, H.: Air pollutant variations in Suzhou
 988 during the 2019 novel coronavirus (COVID-19) lockdown of 2020: High time-resolution
 989 measurements of aerosol chemical compositions and source apportionment, *Environ. Pollut.*, 271,
 990 116298, <https://doi.org/10.1016/j.envpol.2020.116298>, 2021a.
 991 Wang, S. X., Xing, J., Zhao, B., Jang, C., and Hao, J. M.: Effectiveness of national air pollution control
 992 policies on the air quality in metropolitan areas of China, *J. Environ. Sci.*, 26, 13-22,
 993 [https://doi.org/10.1016/S1001-0742\(13\)60381-2](https://doi.org/10.1016/S1001-0742(13)60381-2), 2014.
 994 Wang, Y., Xue, Y. F., Tian, H. Z., Gao, J., Chen, Y., Zhu, C. Y., Liu, H. J., Wang, K., Hua, S. B., Liu, S. H.,
 995 and Shao, P. Y.: Effectiveness of temporary control measures for lowering PM_{2.5} pollution in Beijing
 996 and the implications, *Atmos. Environ.*, 157, 75-83, <https://doi.org/10.1016/j.atmosenv.2017.03.017>,
 997 2017.
 998 Wang, Y. Q., Zhang, X. Y., and Draxler, R.: TrajStat: GIS-based software that uses various trajectory
 999 statistical analysis methods to identify potential sources from long-term air pollution measurement
 1000 data, *Environ. Model. Softw.*, 24, 938-939, <https://doi.org/10.1016/j.envsoft.2009.01.004>, 2009.
 1001 Wang, Y. Y., Liu, B. S., Zhang, Y. F., Dai, Q. L., Song, C. B., Duan, L. Q., Guo, L. L., Zhao, J., Xue, Z.
 1002 G., Bi, X. H., and Feng, Y. C.: Potential health risks of inhaled toxic elements and risk sources during
 1003 different COVID-19 lockdown stages in Linfen, China, *Environ. Pollut.*, 284, 117454,
 1004 <https://doi.org/10.1016/j.envpol.2021.117454>, 2021b.
 1005 Xu, H., Xiao, Z. M., Chen, K., Tang, M., Zheng, N. Y., Li, P., Yang, N., Yang, W., and Deng, X. W.: Spatial
 1006 and temporal distribution, chemical characteristics, and sources of ambient particulate matter in the
 1007 Beijing-Tianjin-Hebei region, *Sci. Total Environ.*, 658, 280-293,
 1008 <https://doi.org/10.1016/j.scitotenv.2018.12.164>, 2019a.
 1009 Xu, L. L., Jiao, L., Hong, Z. Y., Zhang, Y. R., Du, W. J., Wu, X., Chen, Y. T., Deng, J. J., Hong, Y. W., and
 1010 Chen, J. S.: Source identification of PM_{2.5} at a port and an adjacent urban site in a coastal city of
 1011 China: Impact of ship emissions and port activities, *Sci. Total Environ.*, 634, 1205-1213,
 1012 <https://doi.org/10.1016/j.scitotenv.2018.04.087>, 2018.
 1013 Xu, M., Qin, Z. F., Zhang, S. H., and Xie, Y.: Health and economic benefits of clean air policies in China:
 1014 A case study for Beijing-Tianjin-Hebei region, *Environ. Pollut.*, 285, 117525,
 1015 <https://doi.org/10.1016/j.envpol.2021.117525>, 2021.
 1016 Xu, W., Liu, X. J., Liu, L., Dore, A. J., Tang, A., Lu, L., Wu, Q. H., Zhang, Y. Y., Hao, T. X., Pan, Y.
 1017 P., Chen, J. M., and Zhang, F. S.: Impact of emission controls on air quality in Beijing during APEC
 1018 2014: Implications from water-soluble ions and carbonaceous aerosol in PM_{2.5} and their precursors,
 1019 *Atmos. Environ.*, 210, 241-252, <https://doi.org/10.1016/j.atmosenv.2019.04.050>, 2019b.

1020 Yin, H., Liu, C., Hu, Q. H., Liu, T., Wang, S., Gao, M., Xu, S. Q., Zhang, C. X., and Su, W. J.: Opposite
1021 impact of emission reduction during the COVID-19 lockdown period on the surface concentrations of
1022 PM_{2.5} and O₃ in Wuhan, China, *Environ. Pollut.*, 289, 117899,
1023 <https://doi.org/10.1016/j.envpol.2021.117899>, 2021.

1024 Yang, S., Duan, F., Ma, Y., Li, H., Ma, T., Zhu, L., Huang, T., Kimoto, T., and He, K.: Mixed and intensive
1025 haze pollution during the transition period between autumn and winter in Beijing, China, *Sci. Total*
1026 *Environ.*, 711, 134745, <https://doi.org/10.1016/j.scitotenv.2019.134745>, 2020.

1027 Yu, M. F., Zhu, Y., Lin, C. J., Wang, S. X., Xing, J., Jang, C., Huang, J. Z., Huang, J. Y., Jin, J. B., and Yu,
1028 L.: Effects of air pollution control measures on air quality improvement in Guangzhou, China, *J.*
1029 *Environ. Manage.*, 244, 127-137, <https://doi.org/10.1016/j.jenvman.2019.05.046>, 2019.

1030 Zhai, S., Jacob, D. J., Wang, X., Shen, L., Li, K., and Zhang, Y.: Fine particulate matter (PM_{2.5}) trends in
1031 China, 2013–2018: separating contributions from anthropogenic emissions and meteorology, *Atmos.*
1032 *Chem. Phys.*, 19, 11031-11041, <https://doi.org/10.5194/acp-19-11031-2019>, 2019.

1033 Zhang, D. Z., Shi, G. Y., Iwasaka, Y., Hu, M., and Zang, J. Y.: Anthropogenic Calcium Particles Observed
1034 in Beijing and Qingdao, China, *Water, Air, & Soil Pollution: Focus.*, 5, 261-276,
1035 <https://doi.org/10.1007/s11267-005-0743-y>, 2005.

1036 Zhang, Q., He, K. B., and Huo, H.: Cleaning China's air. *Nature*, 484, 161-162,
1037 <https://doi.org/10.1038/484161a>, 2012.

1038 Zhang, Q., Zheng, Y. X., Tong, D., Shao, M., Wang, S. X., Zhang, Y. H., Xu, X. D., Wang, J. N., He,
1039 H., Liu, W. Q., Ding, Y. H., Lei, Y., Li, J. H., Wang, Z. F., Zhang, X. Y., Wang, Y. S., Cheng, J., Liu,
1040 Y., Shi, Q. R., Yan, L., Geng, G. N., Hong, C. P., Li, M., Liu, F., Zheng, B., Cao, J. J., Ding, A. J., Gao,
1041 J., Fu, Q. Y., Huo, J. T., Liu, B. X., Liu, Z. R., Yang, F. M., He, K. B., and Hao, J. M.: Drivers of
1042 improved PM_{2.5} air quality in China from 2013 to 2017, *Proceedings of the National Academy of*
1043 *Sciences*, 116, 24463-24469, <https://doi.org/10.1073/pnas.1907956116>, 2019.

1044 Zhang, Y., Yang, L. X., Bie, S. J., Zhao, T., Huang, Q., Li, J. S., Wang, P. C., Wang, Y. M., and Wang, W.
1045 X.: Chemical compositions and the impact of sea salt in atmospheric PM₁ and PM_{2.5} in the coastal
1046 area, *Atmos. Res.*, 250, 105323, <https://doi.org/10.1016/j.atmosres.2020.105323>, 2021.

1047 Zhao, C. K., Sun, Y., Zhong, Y. P., Xu, S. H., Liang, Y., Liu, S., He, X. D., Zhu, J. H., Shibamoto, T., and
1048 He, M.: Spatio-temporal analysis of urban air pollutants throughout China during 2014–2019, *Air*
1049 *Qual. Atmos. Hlth.*, 14, 1619-1632, <https://doi.org/10.1007/s11869-021-01043-5>, 2021a.

1050 Zhao, S., Tian, H. Z., Luo, L. N., Liu, H. J., Wu, B. B., Liu, S. H., Bai, X. X., Liu, W., Liu, X. Y., Wu, Y.
1051 M., Lin, S. M., Guo, Z. H., Lv, Y. Q., and Xue, Y. F.: Temporal variation characteristics and source
1052 apportionment of metal elements in PM_{2.5} in urban Beijing during 2018–2019, *Environ. Pollut.*, 268,
1053 115856, <https://doi.org/10.1016/j.envpol.2020.115856>, 2021b.

1054 Zong, Z., Wang, X. P., Tian, C. G., Chen, Y. J., Fu, S. F., Qu, L., Ji, L., Li, J., and Zhang, G.: PMF and
1055 PSCF based source apportionment of PM_{2.5} at a regional background site in North China, *Atmos. Res.*,
1056 203, 207-215, <https://doi.org/10.1016/j.atmosres.2017.12.013>, 2018.

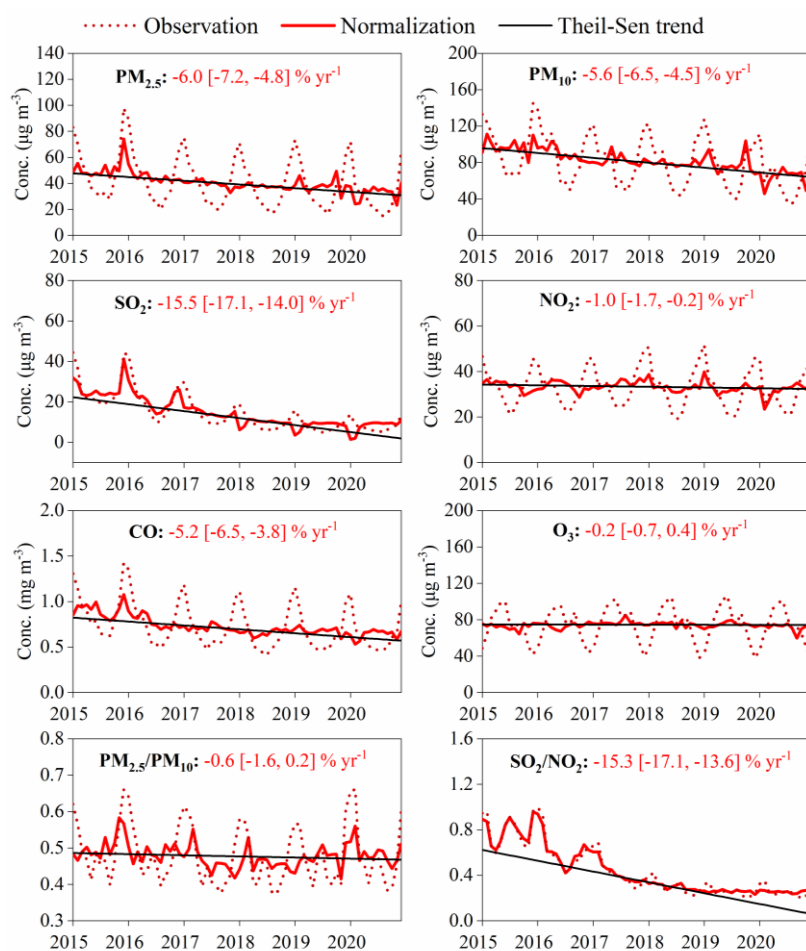


Figure 1. Trends of air pollutant concentrations and PM_{2.5}/PM₁₀ and SO₂/NO₂ from 2015 to 2020. “Observation” represents the observed data, and “Normalization” in represents the modelled concentrations of air pollutants after weather normalization. The black line shows the Theil–Sen trend after weather normalization.

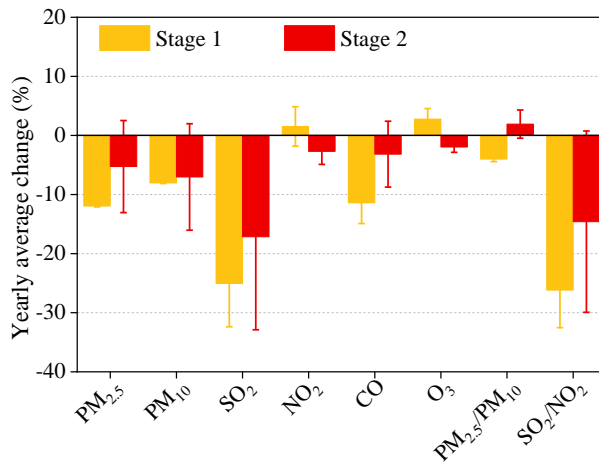


Figure 2. Yearly average change of air pollutants and PM_{2.5}/PM₁₀ and SO₂/NO₂ during different pollution-control stages based on the weather normalized data.

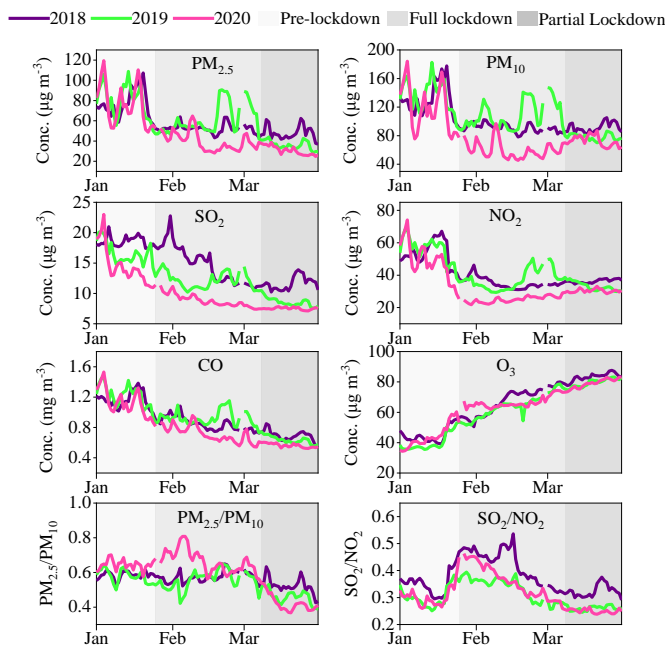


Figure 3. Time series of air pollutants concentrations and PM_{2.5}/PM₁₀ and SO₂/NO₂ during the different stages of COVID-19 lockdown start dates or equivalent in 2020 versus 2018 and 2019 based on the weather normalization data.

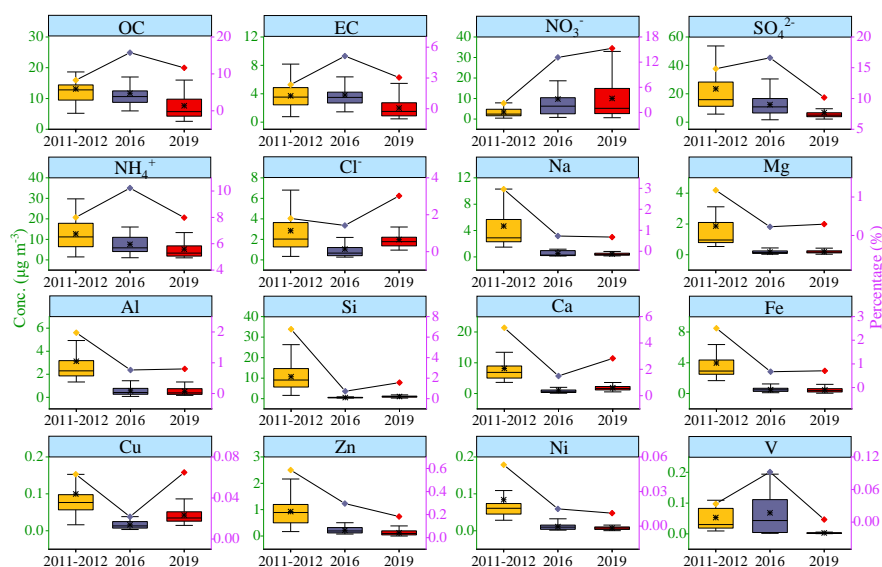


Figure 4. Variations of the average concentrations and percentages of major chemical compositions of PM_{2.5} in 2011-2012, 2016, and 2019. Box charts represent concentrations, and line charts represent percentages.

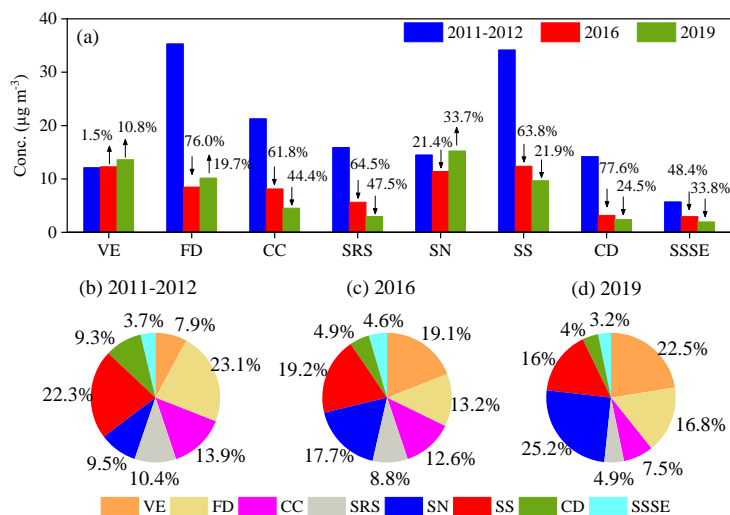


Figure 5. Changes in source contributions for 2011-2012, 2016, and 2019. VE represents vehicle emissions, FD represents fugitive dust, CC represents coal combustion, SRS represents steel-related smelting, SN represents secondary nitrate, SS represents secondary sulphate, CD represents construction dust, and SSSE represents sea salt and ship emissions.

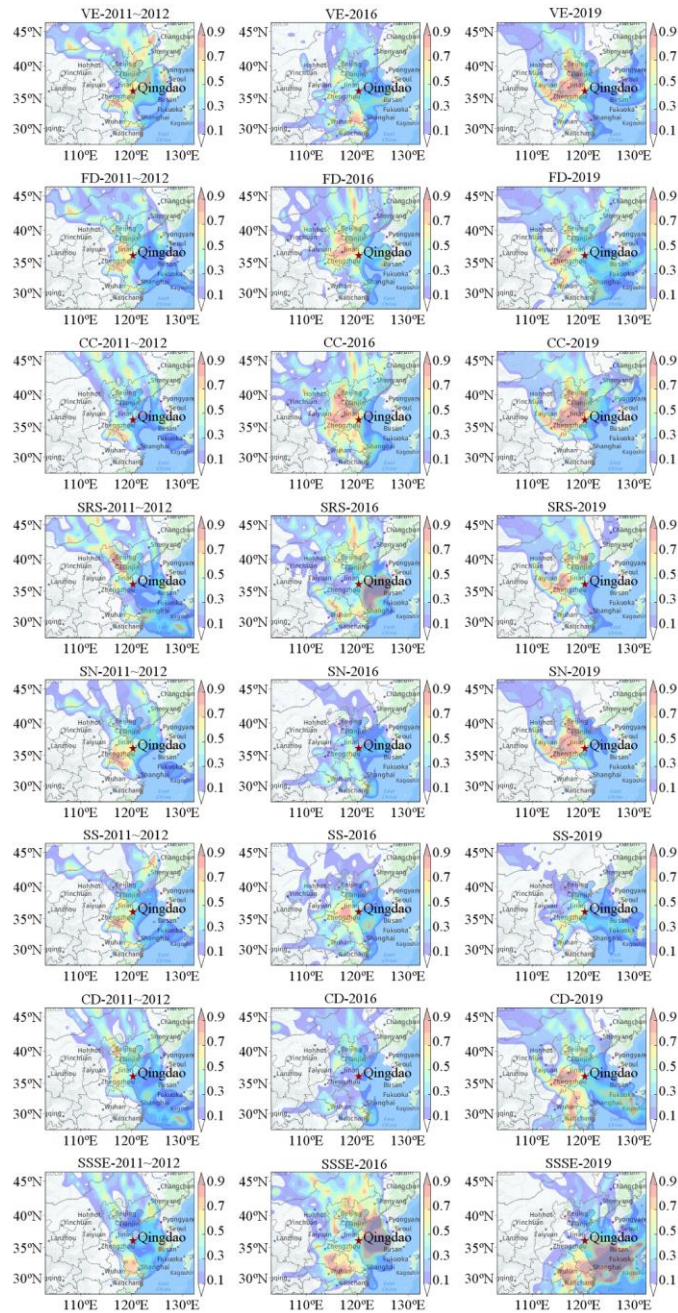


Figure 6. WPSCF plots for various emission sources during different periods (base map from Yahoo Maps). VE represents vehicle emissions, FD represents fugitive dust, CC represents

1090 coal combustion, SRS represents steel-related smelting, SN represents secondary nitrate, SS
1091 represents secondary sulphate, CD represents construction dust, and SSSE represents sea salt
1092 and ship emissions.
1093